UCLA
UCLA Electronic Theses and Dissertations

Title
A Miniaturized Neurostimulator and Recorder with Dynamic Stimulation Capabilities

Permalink
https://escholarship.org/uc/item/7ch050nc

Author
Krishnan, Meghana Asha

Publication Date
2023

Supplemental Material
https://escholarship.org/uc/item/7ch050nc#supplemental

Peer reviewed|Thesis/dissertation

UNIVERSITY OF CALIFORNIA

Los Angeles

A Miniaturized Neurostimulator and Recorder with Dynamic Stimulation Capabilities

A thesis submitted in partial satisfaction

of the requirements for the degree Master of Science

in Bioengineering

by

Meghana Asha Krishnan

2023

ABSTRACT OF THE THESIS

A Miniaturized Neurostimulator and Recorder with Dynamic Stimulation Capabilities

by

Meghana Asha Krishnan

Master of Science in Bioengineering

University of California, Los Angeles, 2023

Professor Wentai Liu, Chair

This work focuses on the miniaturization of a novel bioelectronic stimulator and recorder design into a compact and modularized format that can be implanted into small animals. The feature to allow the dynamic update of stimulation waveforms enables researchers to use this device to mimic the way the nervous system regulates the body.

The dissertation of Meghana Asha Krishnan is approved.

Jun Chen

Jacob J. Schmidt

Wentai Liu, Committee Chair

University of California, Los Angeles

2023

TABLE OF CONTENTS

LIST OF FIGURES

LIST OF TABLES

LIST OF ACRONYMS

ADC   Analog-to-Digital Converter

ANS   Autonomic Nervous System

BLE   Bluetooth Low-Energy

DAC   Digital-to-Analog Converter

ECG   Electrocardiogram

EMG   Electromyography

FBR   Foreign Body Response

GUI   Graphical User Interface

IC   Integrated Circuit

MCU   Microcontroller Unit

PCB   Printed Circuit Board

PNS   Peripheral Nervous System

RTOS   Real-Time Operating System

SCS   Spinal Cord Stimulation

SPI   Serial Peripheral Interface

UART   Universal Asynchronous Receiver/Transmitter

VNS   Vagus Nerve Stimulation

SUPPLEMENTARY MATERIALS

1. Video to demonstrate dynamic update of stimulation parameters. (dynamic_stim_param_update.MOV)

2. Video to demonstrate generation of multiple waveform types. (uart_update_multiple_waveforms.MOV)

3. Video to demonstrate biomimetic signal transfer. (biomimetic_signal_transfer.MOV)

ACKNOWLEDGEMENTS

I would like to thank my thesis advisor Dr. Wentai Liu for giving me this opportunity. His enthusiasm for science is truly infectious, and his knowledge of the field is incomparable. Thank you for sharing your experiences, and for always helping me see the bigger picture.

Yan-Peng Chen, thank you for all your support and mentorship. I could not have done this without your help. You were always ready to answer my endless questions, and you always knew exactly what questions to ask me to make me think further. Thank you for all your effort.

I also want to thank the previous and current members of the Biomimetic Research Lab at UCLA. This work was only possible because of the work that you all did before me, and I'm grateful for the opportunity to learn from such resolute and talented minds.

Finally, I would like to thank my family for all their unconditional support and love. I couldn't have done this without you.

CHAPTER 1: PROPOSAL

1.1 INTRODUCTION AND AIM

Early March 1967, a 70-year-old man arrived at a hospital complaining of severe pain in the chest and abdomen. Dr Norman Shealy, the Chief of Neurosurgery at the Gundersen Clinic in Wisconsin at the time, applied a biphasic electrical stimulation signal to his spinal cord to alleviate the pain. Without any medication, the stimulation was able to eliminate all pain for an hour that day, and nearly 12 hours the next, while still retaining all sensation and mobility.

This treatment has come a long way since then. A wide range of implantable medical devices have evolved from this idea. These devices are used to regulate cardiac dysfunction, recover hearing control inflammation, treat depression, and of course, eliminate chronic pain, among several other applications.

Although the applications are limitless, a lot of fundamental research remains to be done. There is extraordinarily little standardisation in the treatment protocols for specific ailments. Research groups develop their own approaches depending on their focus. There is a need for a device that researchers can use to deepen their understanding of the types of protocols that work, and the mechanisms behind their action.

To further this aim, this project attempts to produce a miniaturised, modular system that can be used for neural signal recording and stimulation. The miniaturised design will enable implantation into small animals, on which most disease models are based. The design can support closed-loop applications by allowing users to dynamically update the stimulation protocol based on their requirements with the hope that this will allow researchers to understand

how best to treat certain diseases, and standardise the "dosage" of stimulation depending on the severity of the disease.

1.3 SCOPE OF THIS WORK

This project builds on the foundational work described in Chapter 2 produced by Yu Nong at the Biomimetic Research Lab in UCLA, under the guidance of Dr. Wentai Liu. The original prototype has been miniaturised into a modularised design that can be that can be used in multiple applications including for implantation into mice. The prototype is currently of the dimensions 8 cm x 3.2 cm, and the miniaturised version is down to 1.2 cm x 1.2 cm in area.

This work also builds upon the previously developed embedded software of the device MCU to add the ability to dynamically update stimulation parameters without stopping any ongoing stimulation, or ensuring that the stimulation remains gapless. The stimulation parameters can be arbitrarily defined by a user and customised extensively. In addition to customised stimulation parameters, the user can also upload a file containing the shape of the waveform of their choice to be uploaded into the device. This feature could be used to replicate the recorded biological-like signals (e.g., EMG) in a biomimetic fashion.

Since this work has been developed as an implantable device, non-invasive methods have not been discussed here. Additionally, the design has been restricted to the electrical hardware and firmware, and other aspects of the design such as the packaging and electrodes have not been addressed here.

CHAPTER 2: BACKGROUND

2.1 BIOELECTRONIC MEDICINE

The terms "Bioelectronic Medicine," "Electroceuticals," and "Neuromodulation" all describe the same idea: the use of electrical stimulation and recording of the nervous system to develop therapies that can treat the body as it would treat itself without administering agents that could provoke an unexpected reaction.

For most people, the first thought that comes to mind when reminded of the functions of the nervous system is the sensation of pain. Since 1967, electrical stimulation has proven to be an effective deterrent to pain - caused either by physical damage to the body (nociceptive) or by damage to the nervous system itself (neuropathic). The medical device industry boasts of several spinal cord stimulation devices (the most prominent companies being Medtronic, Abbott, Boston Scientific, Nevro, and Saluda Medical), that provide targeted electrical stimulation pulses to the spinal cord. Around 30,000 people around the world debilitated by chronic pain undergo implantation each year to go about their lives pain free, at the touch of a button.

The next most evident function of the nervous system would be the ability to transmit and understand the world around us through our sensory organs. It follows that using electrical signals to act as a neural prosthesis in cases where the nerve connected to the sensory organ undergo damage would be the next most common application of electrical stimulation. Cochlear implants are probably the most successful implementation of this idea. The pioneering work of Djourno and Eyries have evolved into the range of products by Advanced Bionics and Cochlear that are used by around 736,900 people worldwide. In a similar vein, there have been multiple attempts over the past three decades to create a commercially viable retinal prosthesis to help

those with visual disabilities. Retina Implant AG and Second Sight Medical Products have helped over five hundred people worldwide, but the complexity and delicacy of the eye as an organ, as well as other economic and technological hurdles have limited development so far [14].

Aside from sensory disabilities, the past 20 years has seen explosive and impactful research into the application of electrical stimulation to manipulate the Autonomic Nervous System (ANS). The ANS is responsible for the regulation of a wide range of organs and tissues, through the central and peripheral nervous systems. These neural networks work interdependently to control cardiac activity, gastrointestinal motility, bladder movement and sensations, immune system operation, and the management of fat in the body, among several other functions. Evidently, the ANS can be used as a pathway to control or limit the progression of a wide range of diseases that affect these functionalities, including, but not limited to, inflammation, cardiac dysfunctions, morbid obesity, and diabetes. In 1997, the FDA approved a vagus nerve stimulation (VNS) system by Cyberonics to reduce epileptic seizures. The device was later approved for the treatment of depression as well, in 2005. With respect to obesity, Enteromedics devised the Maestro Rechargeable System. In a group study conducted by the company, the device caused an additional eight pounds of weight to be lost from the people it was implanted in. Another example of an FDA approved bioelectronic device is Medtronic's InterStim system that targets the sacral nerve to normalise urinary function [13].

The above examples serve to illustrate how electrical stimulation devices have been commercially implemented in the past few decades to create a wide range of medical treatments, and how much more potential remains to be fulfilled. To understand the technical hurdles that lie ahead, an understanding of the basic operation of these devices is required.

2.2 ACTIVATION OF A NERVE FIBRE

A single nerve is composed of multiple nerve fibres, where each fibre may be covered by an insulating layer called the myelin sheath. This layer is not continuous, but is interrupted in multiple locations along the length of the fibre. Each break in the sheath is called a *node of Ranvier*, and forms the primary point of entry and exit for current through the nerve fibre.

Individual neurons within a nerve fibre communicate with each other through electrical changes called *action potentials*. In 1939, Hodgkin and Huxley recorded the shape of an action potential in a squid nerve fibre by inserting an electrode into the nerve and measuring the change in potential across the membrane of the fibre [18]. In a live cell, these action potentials are generated spontaneously in the cell body of the neuron and propagated down the axon to the dendrites, from where they are sent to connecting neurons.
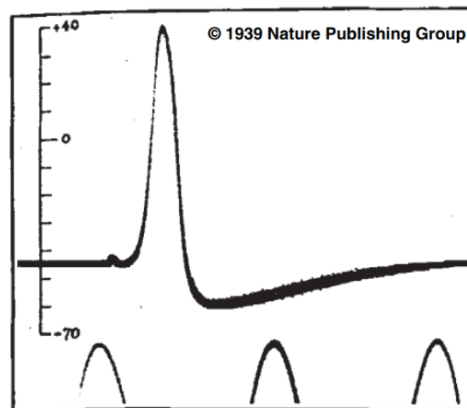
FIGURE 1. Action potential recording from a giant squid axon. The curve depicts the three stages of propagation – depolarisation, or the rapid increase of potential in the positive direction; repolarisation, or the drop in potential from the peak of the spike back to the negative level; hyperpolarisation, or the gradual reduction in the negative overshoot back to pre-depolarisation levels. [18]

The experiment by Ichiji Tasaki in his work *Nervous Transmission* in 1910, describes the behaviour of an isolated motor nerve fibre from a frog when subjected to an electrical current. The "activation" of the nerve fibre was detected by a visible twitch in the frog muscle. A major

5

observation from this experiment was that increasing the electrode current in steps achieved no response until a certain threshold was reached, and that this threshold was also dependant on the direction or phase of the current, and the duration for which it was applied (these aspects will be discussed further in the next section) [17].

It must be noted that increasing the charge delivered to the nerve much beyond the activation threshold can result in an inhibitory effect. When a pulse triggers the depolarisation of a neuron at the stimulation site, there is an equal and opposite hyperpolarisation triggered at another point in the neuron that closes the current loop, and enables the propagation of the action potential. In the case that the delivered pulse is much larger than the activation threshold, a strong depolarising effect is seen, which invokes an equally high hyperpolarisation. This large hyperpolarisation tends to inhibit the propagation of the action potential.

2.3 PARAMETERS OF NEURAL STIMULATION

A stimulation waveform can be broadly described by the template shown in Figure 2. One cycle of stimulation consists of a series of *burst* and *rest* periods. Each burst contains a series of pulses of which the amplitudes and pulse widths can be fixed, or varying.
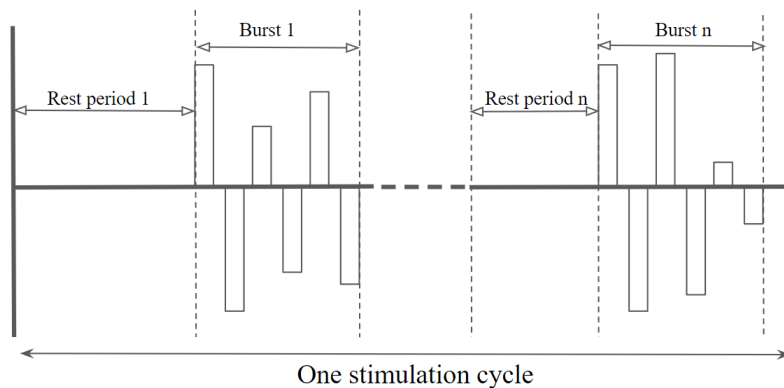
FIGURE 2. General template of a stimulation waveform

IMPACT OF AMPLITUDE AND PULSE WIDTH

The most basic unit of a stimulation waveform is the stimulation pulse. Each pulse is defined by its amplitude and pulse width. The former is most often measured in milliamperes (mA) for current-controlled devices, and Volts for voltage-controlled devices(V), and the latter in microseconds (µs). A pulse of a given amplitude and width is almost always followed by a similar pulse in the opposite direction, in order to balance the total charge delivered to the tissue. Failing to "charge balance" a stimulation pattern can result in the build-up of charge over time which could damage the tissue. Devices that deliver voltage-controlled pulses rely on biological tissue with a constant impedance over time to ensure that the total current delivered is always the same. Current-controlled devices do not suffer from this constraint.

The threshold of activation for a nerve fibre of a given thickness and myelination is proportional to the charge delivered per pulse, which implies that it is the product of amplitude and pulse width of a given pulse that determines a successful activation. This concept is illustrated by the strength-duration curve (Figure 3), which indicates the inverse relationship between amplitude and pulse width for the activation of a nerve fibre [16]. The strength-duration curve tells us how susceptible a fibre is to depolarisation by an external charge, which is also dependent on the thickness of the fibre, its myelination, and distance from the electrode.
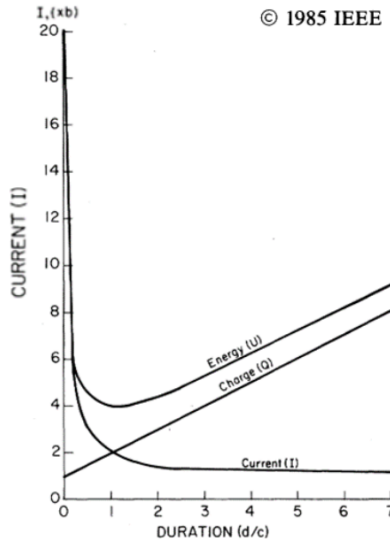
FIGURE 3. The Strength-Duration Curve. 'I' indicates the lowest current that activates the nerve. [16]

IMPACT OF FREQUENCY

The frequency of stimulation defines the number of pulses in a given stimulation waveform, and is thus inversely related to the pulse width. Depending on the application, the chosen frequency can have varied effects. For example, Spinal Cord Stimulation methods traditionally use frequencies in the range of 40-100 Hz. In this range, a mild buzzing sensation (known medically as paresthesia) is produced. However, stimulating at 10kHz can result in pain relief without paresthesia. Since paresthesia requires the activation of specific sensory fibres in the dorsal column, this could mean that high frequency stimulation does not activate these fibres, demonstrating the range of effects observed by just changing the frequency of stimulation [25].

On average, the duration of an action potential for a somatosensory nerve fibre is around 5ms, corresponding to a firing frequency of 200 Hz. This includes the refractory period, or the time taken for the neuron to recover completely. To ensure that neuronal activation is synchronised with the stimulation, a stimulation frequency below the firing frequency is optimal. This

8

frequency is dependent on the type of neuron. As frequencies increase to the kHz range, it is likely that a smaller percentage of nerve fibres in a nerve will be activated, depending on their individual properties. The generated action potentials would then be an unpredictable number, or a response similar to that of a randomised stimulation pattern [12].

IMPACT OF PULSE SHAPES

Ensuring the selectivity of the stimulation is of immense importance to reduce the change of stimulating non-target neurons. Apart from reducing the clinical efficacy, low selectivity could also result in undesired side effects. There may be applications where the desired target either has a lower threshold of activation, or resides deeper in the tissue. In such cases, a standard stimulation pattern could result in the activation of all the fibres with thresholds lower than the target, or those fibres that are closer to the target. One way of mitigating this effect is to add a sub-threshold pre-pulse before the stimulation pulse. The pre-pulse can alter the excitability of non-target fibres, increasing them beyond that of the target. It follows that the subsequent stimulation pulse would then activate only the target fibre [19].

2.4 TECHNICAL CHALLENGES OF IMPLEMENTATION

Bioelectronic medicine is a relatively new field, which implies that there is a huge potential to explore the underlying mechanisms behind neurostimulation. As of now, no standardised procedure for stimulation exists, because most devices are developed based on the specific requirements of individual disease models [20].

Most diseases that are of interest to this field have been modeled on rodents, which makes mice and rat models the best candidates to test the effects and mechanisms of bioelectronic medicine. But there is no device which can be implanted into small animals for long enough to observe the

entire cycle of disease progression and healing. From this observation comes the requirement for a device that can be used for chronic implantation. To facilitate this implantation, additional requirements arise. The device must be small and light enough to be implanted. The Foreign Body Response (the tendency of the body to form an impenetrable layer of tissue around the implanted device over time) to it must be minimal. It should be immune to interference from other bioelectric signals like EMG and ECG, as well as motion artifacts. The device must also be structurally stable if in contact with the Peripheral Nervous System, where there is no rigid foundation to hold on to [20].

In terms of features, a device that can read bioelectric signals while also being able to stimulate nerves would be of utmost use to researchers in this field. In addition to being useful for record-keeping, this allows the device to set stimulation patterns based on these signal readings. This is important because the Foreign Body Response mentioned earlier can reduce the efficiency of stimulation. In such cases, it would be useful to be able to adjust the stimulation intensity or pattern according to the measured signal. There is also the concern of ensuring that the stimulation has the desired effect, and targeting the desired nerve, which can be monitored in a closed loop. The biggest challenges are limiting the size of the device while ensuring that it can behave optimally in all conditions. For mice, the size restrictions are $< 2g$ in weight, and less than $100mm^2$ in area [20].

2.5 STATE OF THE ART

Before describing the work done in this project, it is necessary to obtain an idea of the technology that has been developed already, and what remains to be accomplished. Since this

project focuses on implantable stimulation devices, only invasive devices will be considered in this analysis.

In 2014, Angotzi et al developed a closed loop wireless system for small animals. The system consisted of a backpack containing the main electronic subsystem, and a head stage containing sixteen electrodes, eight for recording and eight for stimulation. The two together comprised the Remote Unit (RU). The RU would connect wirelessly to a Home Unit (HU), which acted as the interface between the RU and a PC that would perform the bulk of the data storage and processing. The closed loop control was designed to detect the number of spikes in the recorded signal and deliver a corresponding stimulus, as well as to react to certain behavioural changes in the animal by providing a stimulus. The RU was powered by a battery with a life cycle of 3 hours. Overall, the ability to perform stimulation and recording over wireless transmission of data was a great achievement. However, the limited battery life would not allow for chronic implantation, and the semi-implanted nature of the device could result in an infection. Additionally, the RU weighed around 40g, which is reasonable for an adult rat of around 300g in weight, but not for a mouse that weighs around 30g.

A novel development in the field appeared in March 2020 in the form of Triangle Biosystems' (TBSI) wirelessly programmable, inductively powered stimulation and recording capsules. The implant can be powered inductively from within 20mm of tissue when the animal is within a wireless cage designed for the purpose. Two variations of a standard biphasic stimulation could be programmed into the capsules. The paper did not specify the size and weight of each capsule, but did describe successful surgical implantations into mice for Vagus Nerve Stimulation. While

the technology is not advanced enough for chronic implantation, these capsules are highly convenient for experiments where wired connections would be difficult to manage [20].

2.6 LIMITATIONS OF THE EXISTING TECHNOLOGY

A review of the literature describing multiple implantable stimulators brings up a few key areas that remain a challenge in the development of a long-term implantable stimulator and recorder.

Most devices rely on the use of a single stimulation pattern for their entire lifetime. Even with systems that use multiple patterns, the limit is usually set to one or two pre-defined waveforms. Few devices allow for a dynamic update of the stimulation waveform, especially waveforms that can be configured and customised by the user. Not only will dynamic updates be useful to change the stimulation to be more effective over the development of the Foreign Body Response that decreases the impact of the stimulation over time; this feature would also allow researchers to examine the effects of multiple types of stimulation parameters and their underlying mechanisms.

Another observation from the review is the restriction of stimulation patterns to biphasic pulsed waveforms, which most often have fixed amplitudes and pulse widths. A standard EMG recording demonstrates how the body uses complex formations of spikes to communicate within itself. Simplifying this intricacy into a standard set of pulses would naturally result in a reduction in the efficacy of the stimulation. It has been demonstrated that using a waveform that mimics this natural signal, or a biomimetic stimulation waveform, produces superior results in the excitability and connectivity of the spinal cord, which could also be used in rehabilitation post trauma [23].

2.7 SOLUTIONS REQUIRED

As described earlier, the existence of multiple disease models based on mice necessitates the development of a device that can enable researchers in the field of bioelectronic medicine to test various stimulation paradigms and understand the biological mechanisms behind their operation. For this application, the most important aim would be to miniaturise existing solutions into forms that can be implanted safely and long term, in mice.

Additionally, this application would need to enable the continuous update of stimulation waveforms while ensuring that the ongoing stimulation remains continuous to ensure that there is no disruption to the experimental protocol. The stimulation protocols must not be restricted to a few basic patterns, but must be configurable over a wide range of parameters. Furthermore, the ability to update the device with a biomimetic stimulation pattern would be essential to replicating the natural control mechanism of the body.

2.8 OVERVIEW OF FOUNDATIONAL WORK

This section contains a description of the system developed by Yu Nong and Yan-Peng Chen in the Biomimetic Research Lab at UCLA, under the guidance of Dr. Wentai Liu.

SYSTEM ARCHITECTURE

The system can be separated into three main parts: the implant consisting of the stimulator, recorder, power circuitry and MCU; the backend PC where the user enters parameters and specifications through a custom GUI, and the adapter that process commands from the backend GUI and converts them into BLE signals to send to the implant. The entire architecture is shown in Figure 4.
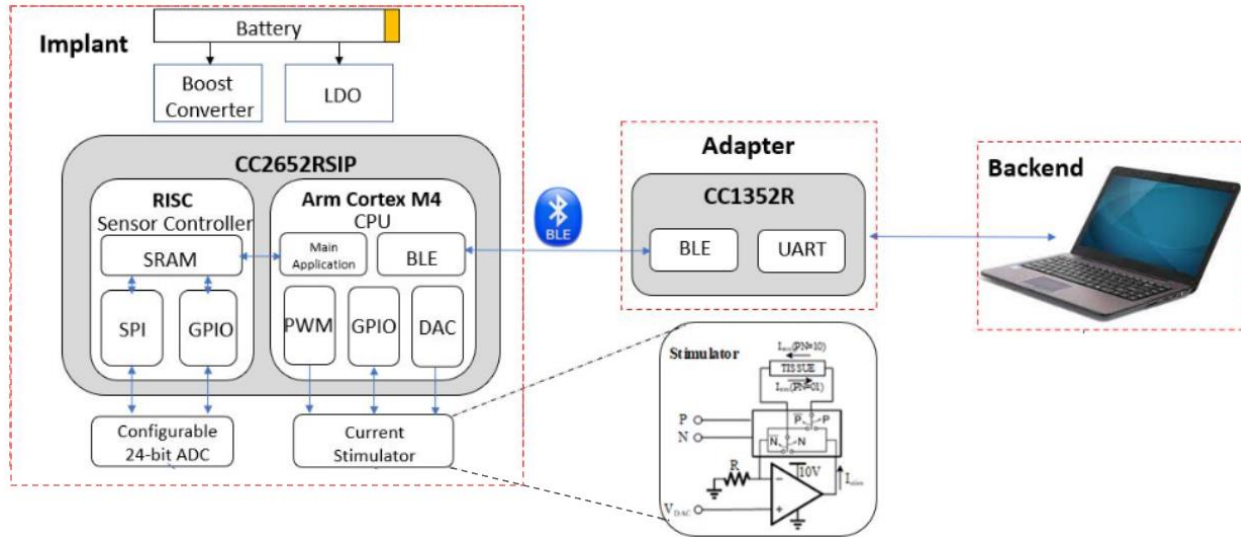
FIGURE 4. System architecture. [24]

Note: Since this thesis focuses mainly on the miniaturisation of the hardware, the development of the wired UART connection, and the addition of features to the MCU, aspects from the foundational work such as the BLE system, stimulation artifact cancellation, and the GUI will not be described in this work. Readers can refer to the extensive documentation of this foundational work in the Thesis Dissertation by Yu Nong, published 2022 [24].

HARDWARE

The hardware design of the implant is separated into three modules: the power module, the stimulator module, and the recording module.
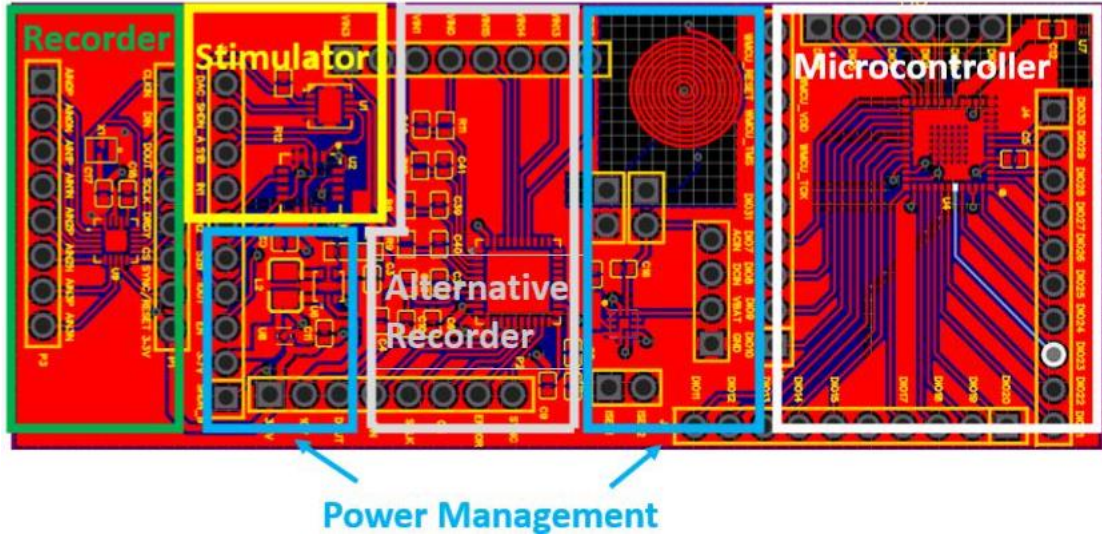
FIGURE 5. PCB layout of implant. [24]

POWER MODULE

The power module receives wireless power from an external transmission circuit and converts it into a DC voltage, which is used to charge a battery on the implant. The wireless charging is performed by a receiver coil created by a PCB trace, and the IC LTC4124 which converts the received AC voltage from the coil into a DC output to power the implant.

Power for the digital MCU and ADC comes from the TPS7A0233PDQNR low drop-out IC, which converts the DC output from the LTC4124 to a 3.3V supply. The stimulator module is powered by a LTC3459EDC#TRMPBF boost converter which produces a 10 V output [24].

Parameter	Value
DC Output from wireless charger	3.3 V – 4.5 V
Maximum current consumption	15 mA
Battery capacity	600 mAh
Battery lifetime	40 hr at maximum current

TABLE 1. Power module specifications [24]

15

Stimulation is achieved by the low power op amp LT1637 as a voltage controlled current source. The output current generated with a single polarity. Before the current passes through the load (tissue to be stimulated), the switch ADG5436 determines its final polarity, controlled by GPIOs from the MCU.
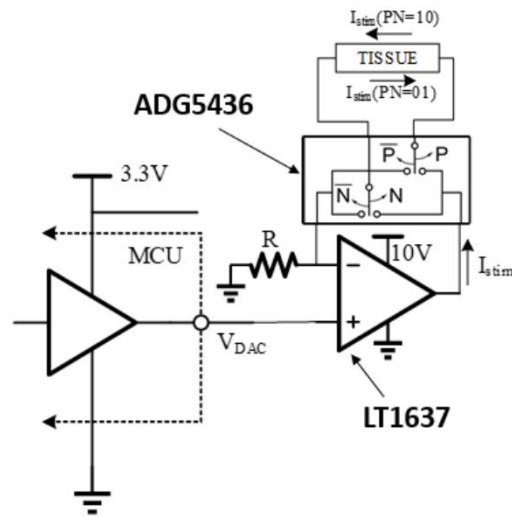
FIGURE 6. Stimulator module [24]

Various current levels are achieved by the conversion of the output DAC voltage from the MCU into a constant current, through the formula $I_{stim} = \frac{V_{DAC}}{R}$ (1).

Parameter	Value
Maximum Current Output	2 mA (R = 500Ω)
V_{DAC} resolution	12.8 mV
I_{stim} resolution	7.8 μA

TABLE 2. Stimulator module specifications [24]

RECORDING MODULE

The ADS131M04 IC was used as the recording ADC due its small package size (3.00mm x 3.00mm) and its programmable gain up to 128. The ADC provides four differential recording channels at 24-bit resolution, although only a single channel was implemented in this design. This system does not provide the dedicated clock at 8.192 MHz, but instead uses a clock at 8 MHz from the MCU, which reduces the sampling rate of the ADC [24].

MCU AND FIRMWARE

The CC26x2 is a low-power MCU with wireless BLE, as well as wired SPI and UART capabilities. The MCU has an integrated 48 MHz crystal oscillator that greatly reduces its footprint on the PCB in comparison to its predecessors.

Since the MCU functions on a single core, the Texas Instruments real-time operating system (TI-RTOS) is used to juggle multiple tasks across clock cycles.

The features and specifications of the MCU have been described in Figure 7 on the next page.
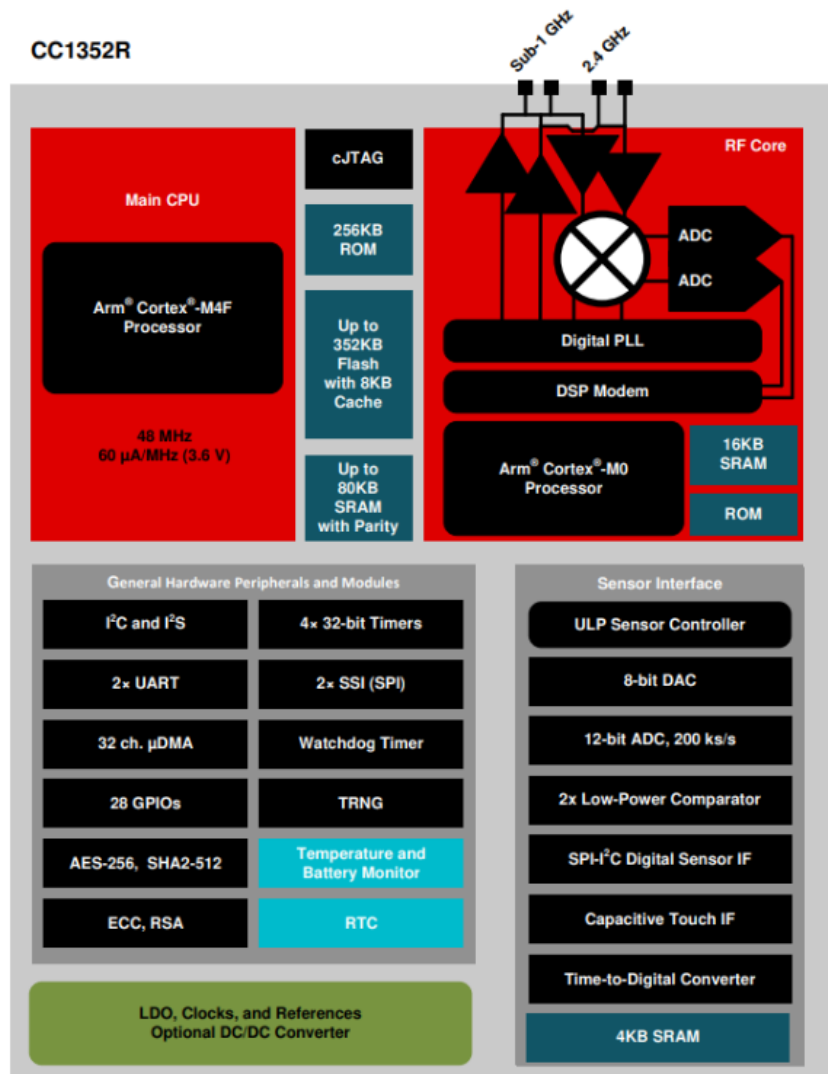
FIGURE 7. Overview of CC2652RSIP MCU. [24]

As mentioned, the TI-RTOS manages three main tasks: stimulation, BLE, and recording. The

stimulation task sets the amplitude, pulse widths, and polarity of each stimulation pulse in the

defined pattern, by providing the DAC output and switch polarities to the stimulator module in

the implant. The recording task monitors the readings from the ADC, and sends this data through

BLE to the external adapter. The BLE task checks for commands from the BLE adapter that

arrive from the backend GUI, and use these commands to modify stimulation parameters. The

recording task has the highest priority, with the BLE task coming second, and the stimulation

task coming last in order to eliminate the loss of data during the transfer [24].
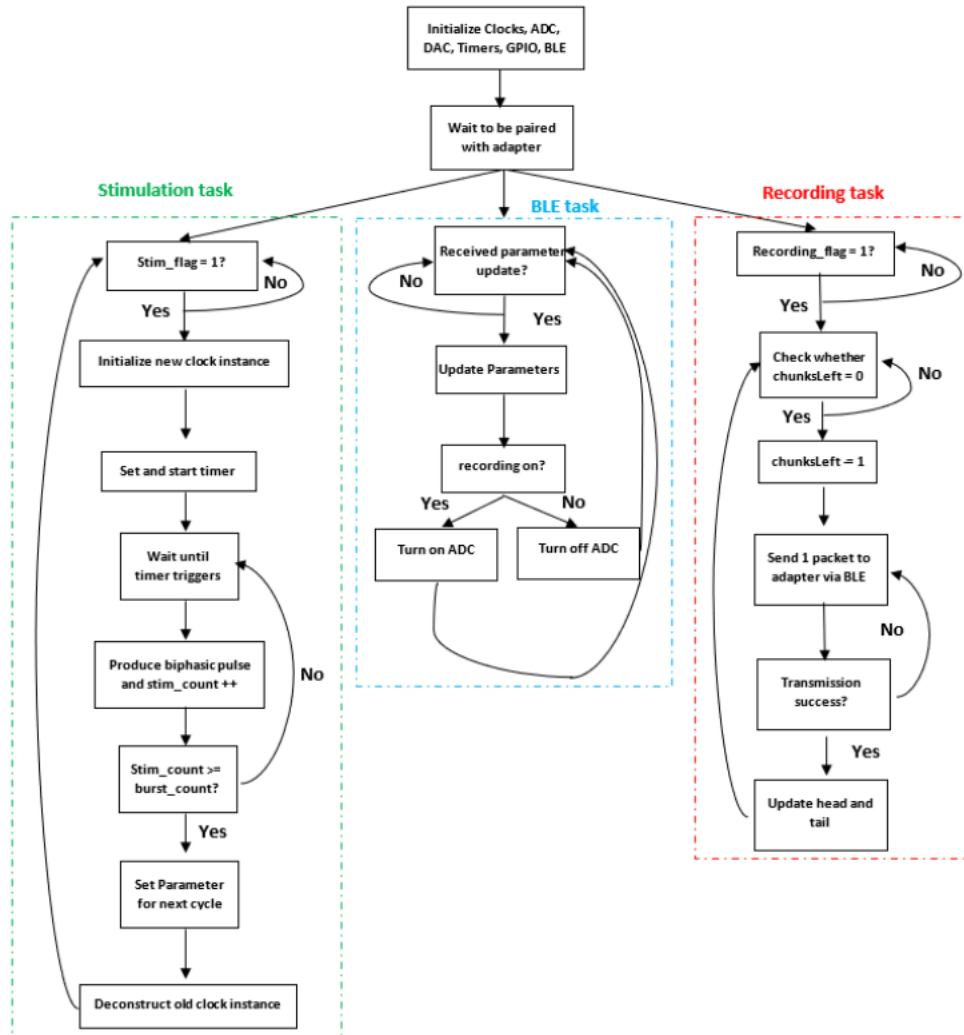
FIGURE 8. Flowchart of tasks in firmware.[24]

CHAPTER 3: MINIATURISATION OF REMOTE SYSTEM

The limitation of the foundational design is the size, which is 8cm x 3.2 cm in area. This indicated that the main aspect of improvement would be to reduce the size to within the desired limit, while retaining functionality and ensuring signal integrity.

Miniaturisation was accomplished by splitting the original PCB layout (Figure 9) into three boards, dividing the functionality between each board. It was decided that the layout would be split into three 12mm x 12mm boards: one with the ADC and the MCU unit, another with the stimulator circuit and power modulation, and the last one for wireless power transfer with the PCB coil and the wireless charging IC. The implant, or the remote system can be separately configured or updated for different applications.

The total height of the board can be calculated using the thickness of each individual board, and height of the board-to-board connectors. The thickness of each board is 0.8mm. Between Board 1 and 2, the connector BC020 and BC035 of heights 1.2mm can be used, and the connector BC084 of height 2.25mm is used between Boards 2 and 3. This produces a total height of 5.85mm.
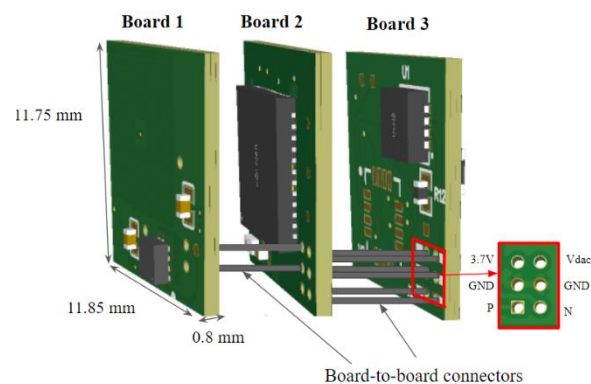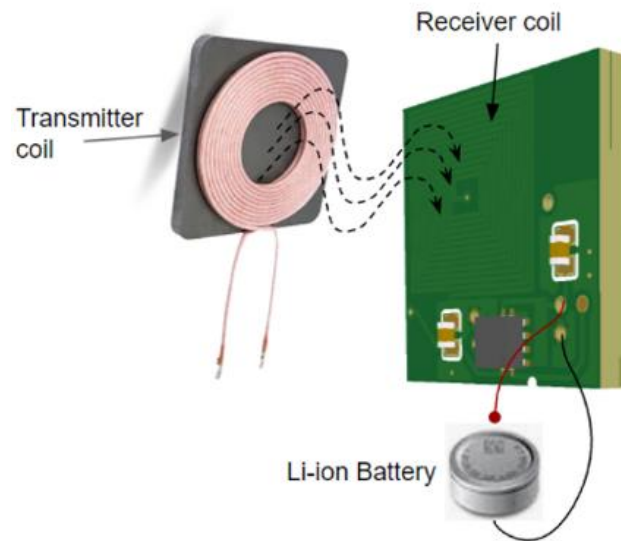

FIGURE 9. Board-to-board connections of remote system.
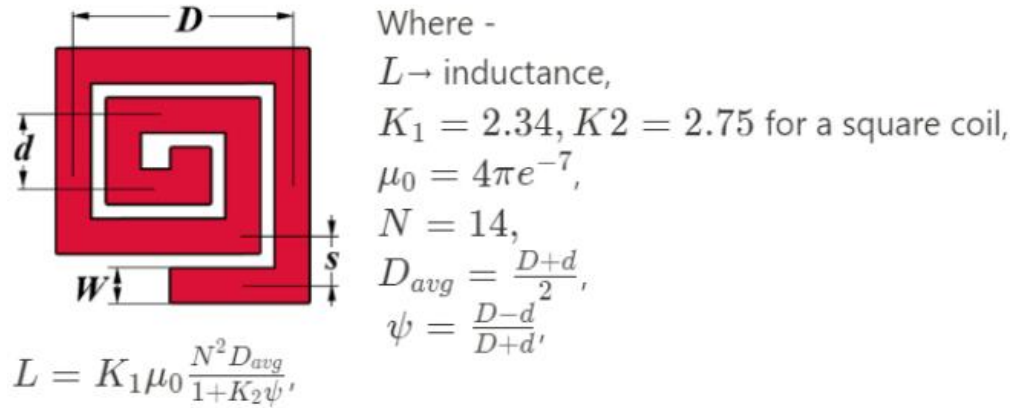
3.1 BOARD 1: POWER

Board 1 is a modified version of the power module from the foundational design. In this design, the dimensions of the receiver coil PCB trace were modified to produce a higher inductance value in order to optimise the wireless power transmission.

FIGURE 10. Operation of power board.

The receiver coil was split from a single layer into a two-layer PCB trace inductance. The copper plane below the coil was removed to maximise inductance, which meant that no traces could be routed in this region.

The equation for the inductance of a PCB trace is given in Figure 11. The equations have been taken from an online PCB coil calculator program [26]. This design uses a square coil shape as opposed to the circular shape used in the foundational design, because the K_1 and K_2 coefficients are larger with the square shape, providing a larger inductance for the same area.
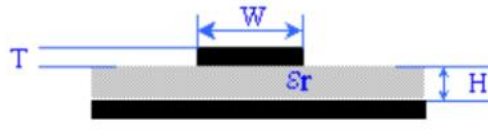
Where -
$L \rightarrow$ inductance,
$K_1 = 2.34, K2 = 2.75$ for a square coil,
$\mu_0 = 4\pi e^{-7}$,
$N = 14$,
$D_{avg} = \frac{D+d}{2}$,
$\psi = \frac{D-d}{D+d}$,

$$L = K_1 \mu_0 \frac{N^2 D_{avg}}{1+K_2\psi},$$

FIGURE 11. Inductance of a square coil.

As per the PCB layout design, D = 7.6 mm, d = 0.45 mm, W = 0.2mm, and s = 0.2mm. Using the coil dimensions in the formula in Figure 11 gives an estimated inductance of 0.67μH on each side, amounting to 1.34μH in total.

The parallel resonant tank for the LTC4124 was designed for the specification of 6.56 MHz frequency. The self-resonant frequency of an inductor is the frequency at which the parasitic capacitance of the inductor resonates with the ideal inductance. Inductors operate as inductors only until the self-resonance value. This means that the desired specification of 6.56MHz must be less than this value. The self-resonant frequency is calculated as $f_{res} = \frac{1}{2\pi\sqrt{LC}}$, where L and C are the self-inductances and self-capacitances of the inductor, respectively.

To obtain this frequency, the self-capacitance must first be obtained. The self-capacitance of the PCB coil trace is calculated from the formula in Figure 12, obtained from an online calculator program [27].

22

$$C_o = \frac{0.67(\varepsilon_r + 1.41)}{\ln\left(\dfrac{5.98H}{0.8W + T}\right)} \text{ pF/inch}$$

FIGURE 12. Self-capacitance of a microstrip. [27]

From the design dimensions, H = 0.8mm, W = 0.2mm, T = 0.2mm, and ε_r = 5.5. This gives a self-capacitance of 0.7pF/cm, or 33pF for 47 cm, which is the total length of the coil. This is an approximate calculation, but the results give an estimation for the parasitic capacitance of the coil. This value of self-capacitance results in a self-resonance frequency of 24 MHz, which is much larger than the chosen frequency of 6.56MHz, and so the inductor design will operate as an inductance for the chosen frequency.

For the chosen frequency of 6.5Hz, a total capacitance of 0.4nF is required. To tune the resonance to a precise value, it is recommended that the capacitor chosen to be of a variable capacitance to accommodate for parasitics in the layout.

The transmission circuit was simulated in LTSpice (Figure 13) to determine the optimum values of the parallel resonant tank on the transmission side.
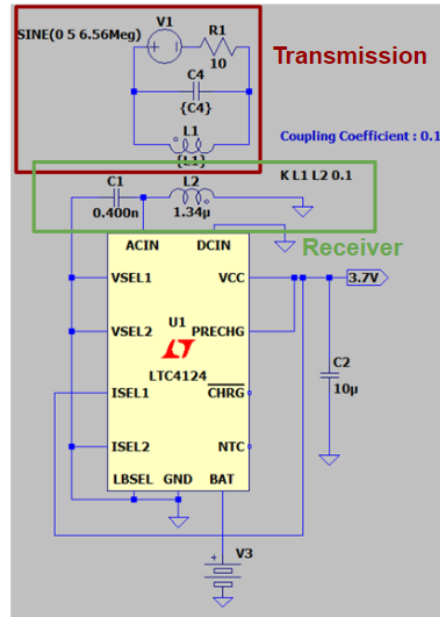
FIGURE 13. LTSpice circuit simulation of wireless transmission and receiver

It was seen that when a 10µH primary coil driven by a 15V, 6.78MHz sinewave was coupled

with a coupling coefficient k=0.1 (perfect coupling would have k=1, and 0 where the two coils

do not interact at all) to the receiver coil, the wireless charger received enough power to regulate

its output to 3.6V as shown in the figure below. The coupling coefficient is typically within the

range of 0.3-0.6, but a value of 0.1 was chosen to demonstrate the worst-case simulation. The

ripple at the output of the wireless powering chip with a 10uF output decoupling capacitor is

simulated to be 50mV.
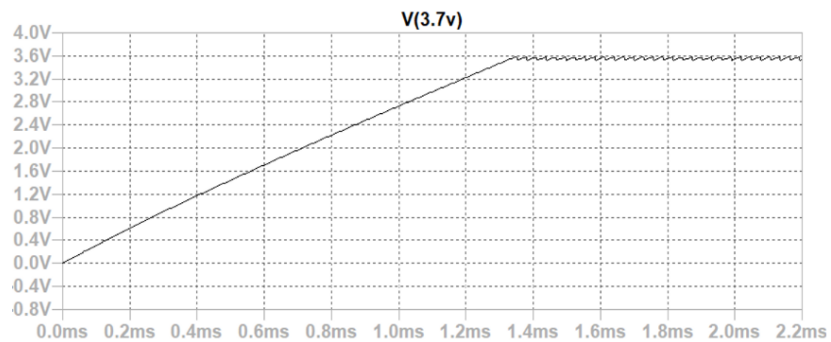
FIGURE 14. Simulation result of the regulating performance of the wireless battery charger when the 10µH transmitter coil was driven by a 15V, 6.78MHz sinewave with a coupling coefficient of 0.1 to the receiver coil.

24

Figure 15 depicts a visualisation of the PCB layout of Board 1 from the top and bottom.
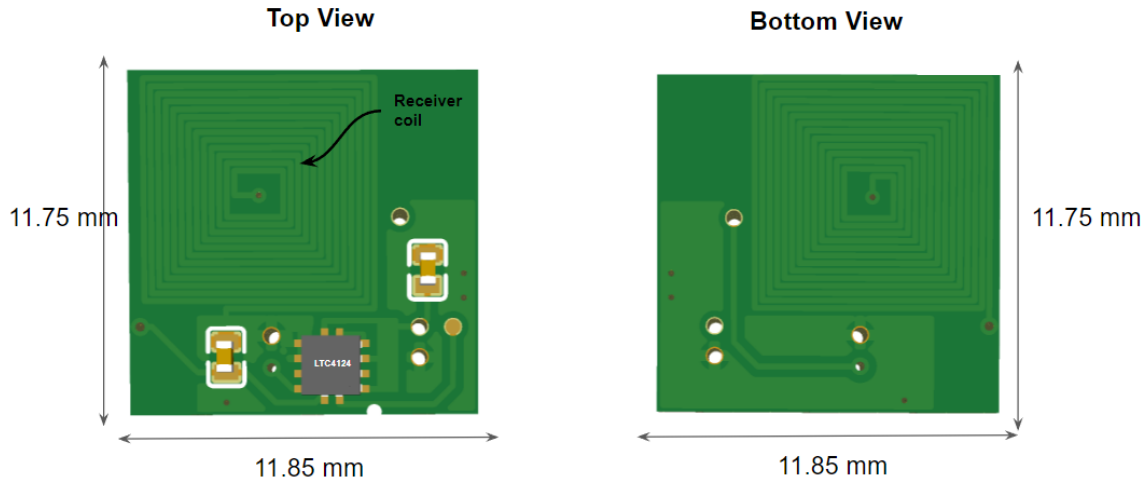
FIGURE 15. 3D render of Board 1 PCB layout

For applications requiring compact rechargeable batteries, Li-ion batteries are an ideal choice.

Some possible products that are compatible with the implant system are shown in the table

below.

Model Name	Capacity	Voltage	Dimensions
GP1258-05N	56mAh	3.6V	12.1 mm dia, 5.85 mm ht
LPM1054	50mAh	3.8V	5.4 mm dia, 10 mm ht

TABLE 3. Suitable battery models and specifications.
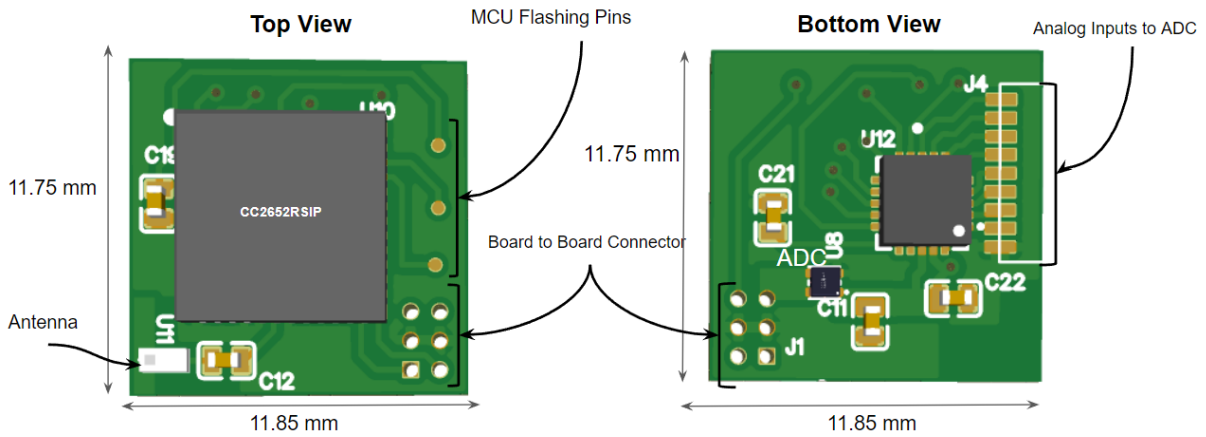
3.2 BOARD 2: CONTROLLER AND RECORDING

The main components on Board 2 are the 3.3V regulator (TPS7A0233), an MCU (CC2652RSIP)

with an antenna, an ADC (ADS131M04), and a chip antenna (ANT016008LCS). The ADC

communicates with the MCU with a four-wire SPI interface through PCB interconnects. The

short connection minimizes the chance of data corruption and mishandling of registers. Two

additional layers of the ground plane are added in-between ADC and MCU to shield the switching noise of the MCU from the acquired signal. Once the data is transferred, the neural signal is buffered into the remote device and wirelessly streamed to the laptop/computer without data loss.
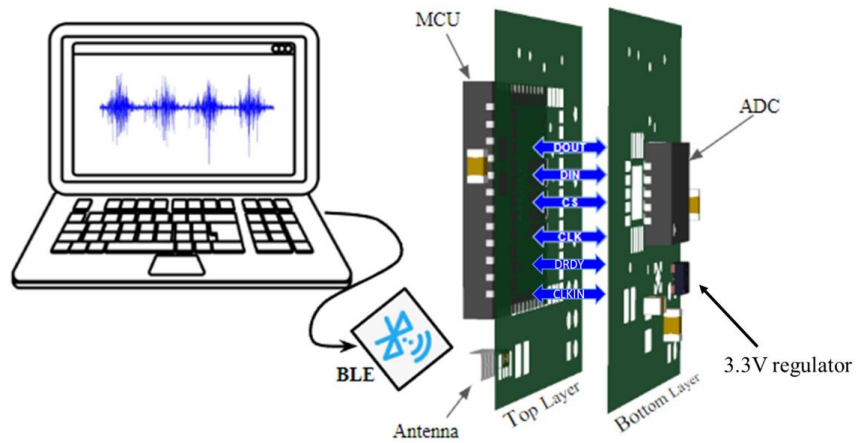
FIGURE 16. Wireless communication between the controller and recording board.

Figure 17 shows a visualisation of the final PCB layout for Board 2.

FIGURE 17. 3D render of Controller and Recording board PCB layout.

3.3 BOARD 3: STIMULATOR

Board 3 comprises the stimulator module described in Chapter 4 on one side, and the LTC3459 boost converter circuit on the other to provide the necessary supply to the op-amp circuit.

A simulation of the stimulator board was created in LTSpice, as shown in Figure 18. The simulation was used to generate a 5mA biphasic pulse train (cathodic first) of 180ms active time and 320ms inactive time, with a pulse width of 4ms. The load is a Randles cell model of the cell membrane capacitance and tissue resistance.
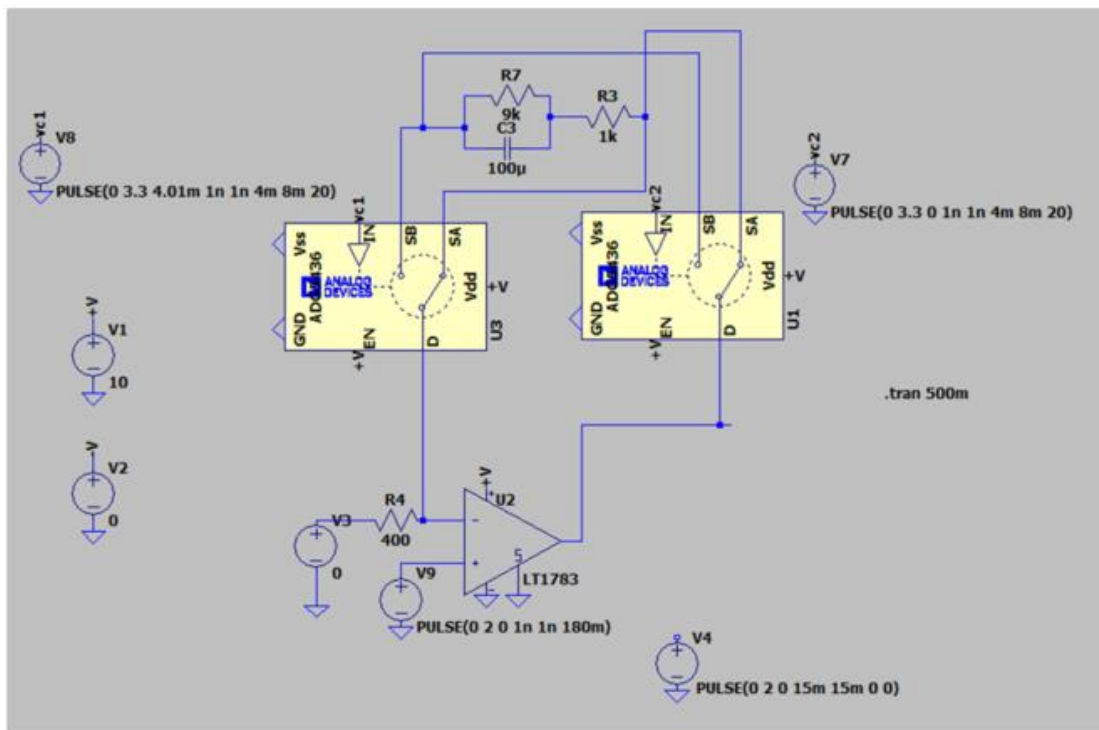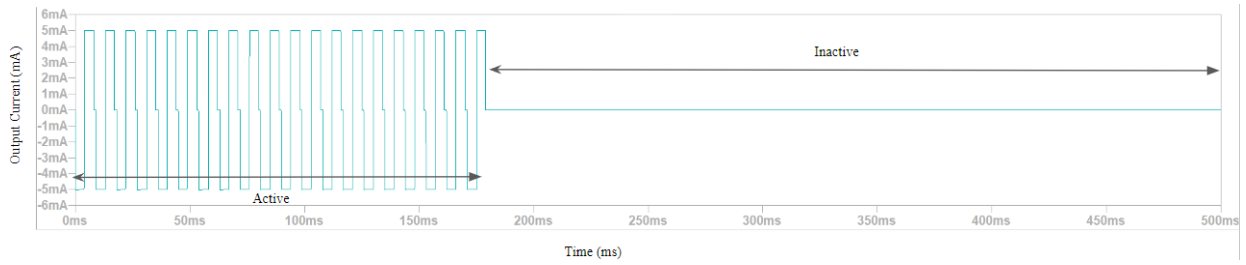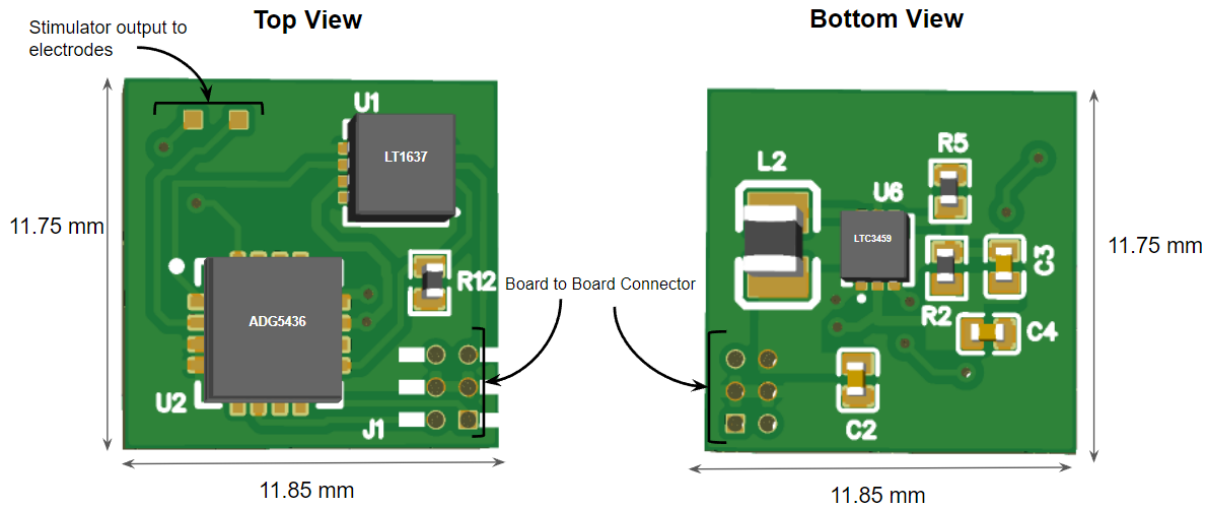

FIGURE 18. LTSpice simulation of the stimulator circuit.

The output current of the stimulator is as seen in Figure 19.

FIGURE 19. Output of stimulator simulation.

Figure 20 depicts a visualisation of the PCB layout of Board 3.

**FIGURE 20.** 3D render of the Stimulator board PCB layout.

CHAPTER 4: DYNAMIC UPDATE OF STIMULATION

This chapter describes the second half of the project: the dynamic update of stimulation parameters that enables users to customise stimulation as per their application. For this project, the implementation of dynamic stimulation was done over a wired UART connection. Although wired connections limit mobility to within the range of the wires and does not allow complete implantation, it is more suitable for an experimental device due to the versatility of its configuration that enables faster and simpler troubleshooting.

A UART connection when optimised to its limit, presents the fastest way of transferring a large amount of data into the device. Although this is aspect is presented as a limitation here, the constraint is presented by the specifications of the chosen MCU model, and not the UART interface.

The customised stimulation can be created in two ways by the user, as depicted in Figure 21:

1. The user specifies individual parameters that make up a stimulation waveform. The parameters are then sent over UART, and the MCU uses them to generate a stimulation waveform.
2. The user uploads a file containing waveform datapoints at fixed timestamps. The UART interface first transfers the duration between each data point (which forms the pulse width), then transfers the waveform datapoints, and the MCU uses these values to create a corresponding stimulation waveform.
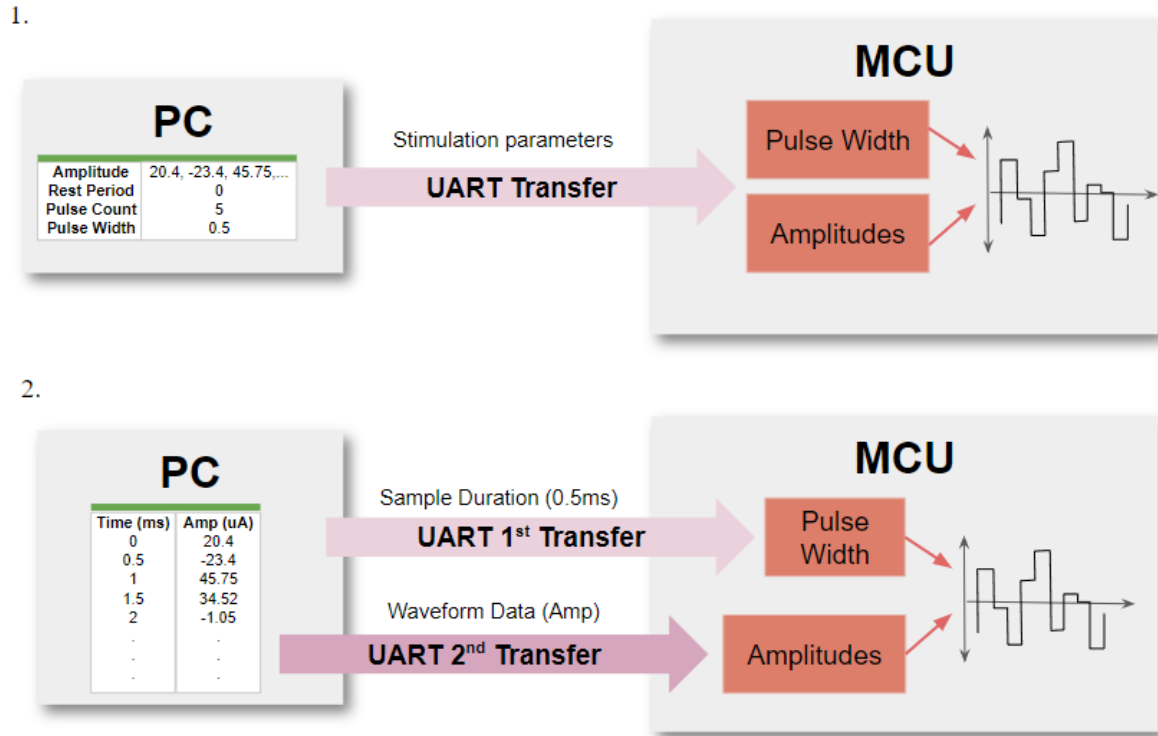
FIGURE 21. Two ways to generate customised stimulation waveforms.

4.1 UART INTERFACE BETWEEN PC AND MCU

UNIVERSAL ASYNCHRONOUS RECEIVER/TRANSMITTER (UART)

UART is a serial communication protocol that requires only two wires between communicating devices since asynchronous communication does not require an extra clock signal. Instead, the transmitter and receiver are configured to operate at the same speed, and the data transfer is detected by start and stop bits that "frame" the data. This implementation uses the 8N1 configuration, with 1 start bit, 1 stop bit, and no parity bit. The baud rate chosen was 2Mbps. The data frame for this configuration is depicted in Figure 22.
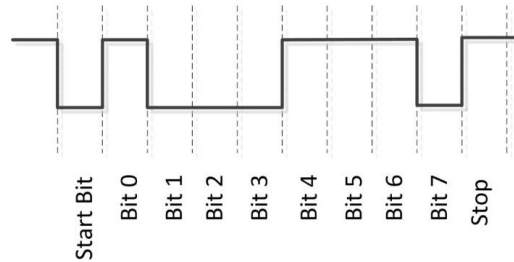
FIGURE 22. UART data frame in 8N1 configuration

INTERFACE BETWEEN PC AND MCU

The sequence of events depicted in the block diagram are described below, and in Figure 23.

A. User Input

1. The user creates an input file. This file can either contain stimulation parameters (file Type-1), or a sequence of data points as waveform data (file Type-2).

2. The user runs the Python program. The program asks for the name of the input file, and the user enters the created file name.

B. Python Program

1. The Python program (uart_mcu_comm.py) reads the user input file, and detects the file format to be either of Type-1 or Type-2.

2. The program opens a UART serial port with the 8N1 configuration and a baud rate of 2Mbps with the help of the PySerial library.

3. If the file is detected to be of Type-1:

   a. The python program iterates through the parameter types (amplitude, pulse width, etc)

   b. For each parameter type, the program collects the parameter values and sends them over the UART interface.

4. If the file is detected to be of Type-2:

31

a. The program calls another script (file_parse.py) to process the waveform data, and passes the input file to this new script.

b. file_parse.py detects the length of the data in the file. If the length is less than 100 values, the program simply converts this file into the desired format by transposing the data in the file. This makes sure that the first line in the file contains all the data in the file.

c. If the length of the data file is greater than 100, file_parse.py splits up the datapoints into blocks of 100 values, and then writes each block line-by-line into the output file, such that each line contains 100 values.

d. Once file_parse.py has run, the original program uart_mcu_comm.py reads the generated output file line-by-line. Each line is then sent as a single block over the UART interface.
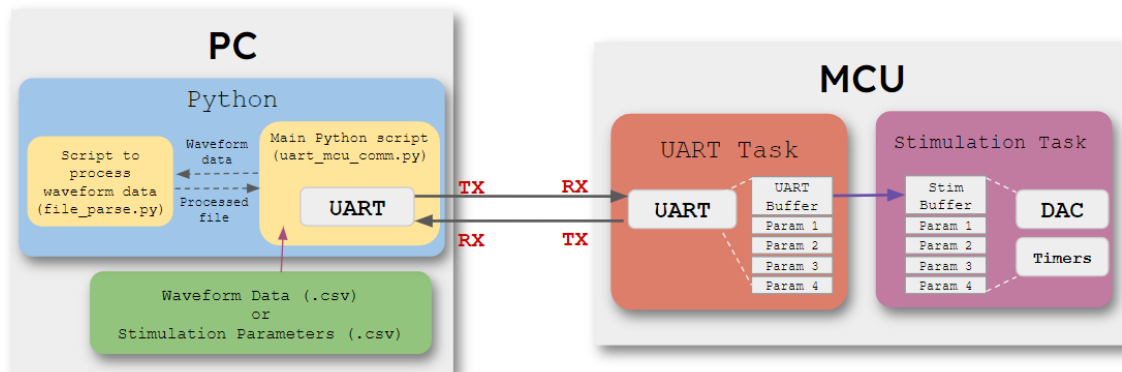
FIGURE 23. UART interface between PC and MCU

4.2 ORGANISATION OF MCU FIRMWARE

As described in section 2.8, the MCU runs a stimulation task and a communication task in separate threads. The TI-RTOS manages the processor load, and decides which thread is to be performed in each clock cycle, based on the assigned priorities of each task. A new UART task

thread that runs in parallel with the stimulation task was created for this purpose. The UART task is given a lower priority, since it is essential that stimulation continues to run smoothly irrespective of an ongoing UART update.

STIMULATION PARAMETERS

Section 2.8 depicted the general template of a stimulation waveform. Any waveform can be configured from the parameters described, as shown in Figure 23. The parameters are presented in detail in Table 4.

Parameter	Description
Stimulation Cycle (us)	Total period of stimulation waveform
Burst	A series of pulses in a defined pattern
Rest period (us)	Duration of inactivity between bursts
Pulse Amplitude (mA)	Amplitude of each pulse in a burst
Pulse Width (us)	Width of pulses in each burst
Inter-Pulse Delay (us)	Delay between pulses in each burst
Pulse Count	Number of pulses in each burst
Burst Count	Number of burst and rest periods in a stimulation cycle
Stim Count	Number of stimulation cycles

TABLE 4. Descriptions of stimulation parameters.
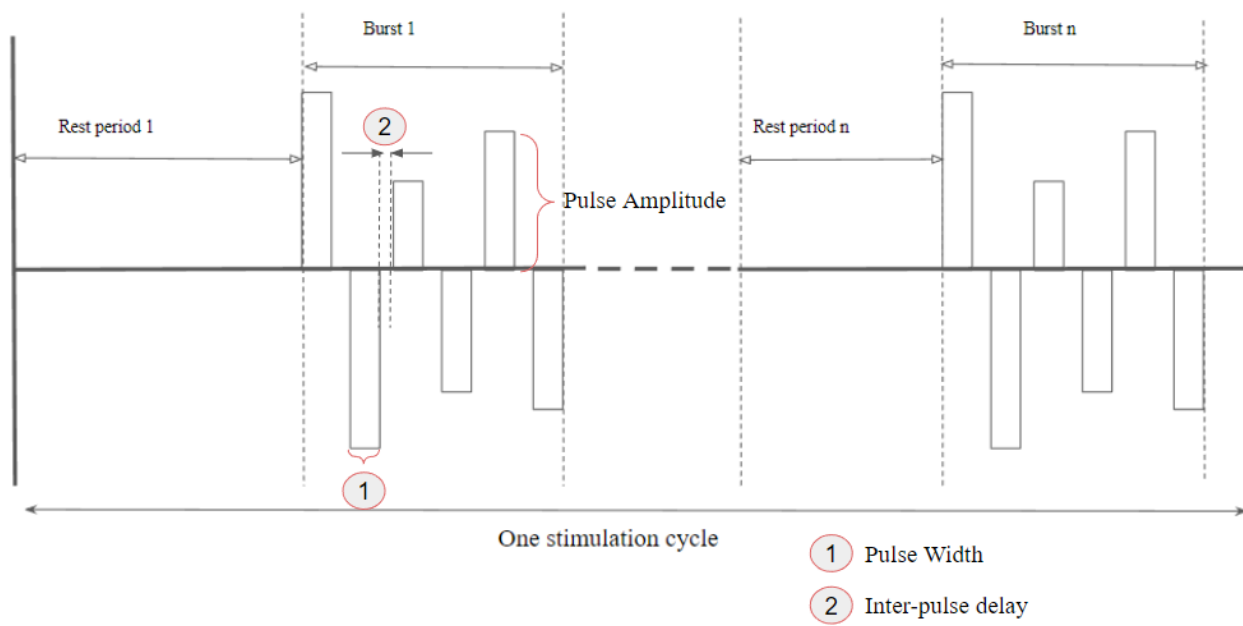
FIGURE 24. Stimulation parameters.

The stimulation parameters are stored as integer (int16_t, or 2-byte per integer) arrays in the MCU. The length of each array is set to a maximum of 100 values in the current version of firmware.

INTEGRATION OF UART DATA WITH STIMULATION

Figure 8 in section 2.8 describes the flow of the stimulation task in the MCU, and how the stored stimulation parameters are used to update the stimulation cycle. This process of generating each burst remains the same. The additional feature is the introduction of a UART task thread (shown in Figure 23) that runs along with the stimulation task, checking the UART receive buffer for new data.

The Tx and Rx pins in the MCU hardware are pulled high during the idle state. When a start bit is sent (Figure 22), it causes the Rx line to be pulled down, signalling the arrival of new data. The data bits that arrive after the start bit are read into the UART Rx buffer.

The Rx buffer is implemented in a ring configuration with a predefined size. The "head" and "tail" positions of the ring buffer are stored in the MCU. As new data arrives through the Rx line, it is written into the Rx ring buffer, starting with the head position. If the tail position is reached before all the new data is written into the buffer, the remaining data begins overwriting the data at the head. This continues in a circular fashion until all the new data has been read, as shown in Figure 25.
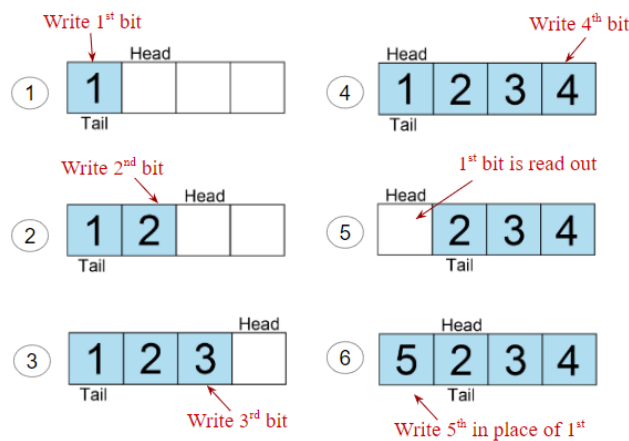
FIGURE 25. UART Rx FIFO ring buffer operation. 1, 2, 3, and 4 depict the writing of 4 bits into the buffer of size 4. If another bit is written into the buffer beyond this, it will be written at the current head position (overwriting value 1). Instead, if the bit at the head position is read out of the buffer by the program, the new bit can take its place at the head as shown in 6.

To ensure that data that has been written into the buffer is not overwritten by new data, the buffer length is increased to accommodate the largest size of the incoming input data.

Once the incoming data has been read from the UART buffer, it is stored in a temporary array. This is to ensure that the existing stimulation parameters are not overwritten until the ongoing stimulation has completed. Once the ongoing stimulation has completed, a flag is set to transfer the data from the temporary array into the stimulation parameter array. Beyond this, the stimulation proceeds in the regular manner.

CHAPTER 5: RESULTS

This chapter depicts the outputs of the features added to the MCU firmware.

5.1. SETUP

Testing was carried out on the CC1352R1 Launchpad, which also supports firmware for the CC2652R1 MCU chip. The Launchpad connects to the PC through a micro-USB to USB-A connection, through which the UART transfer is performed. The DAC and GPIO outputs from the MCU are connector to another circuit board on which the stimulator module has been created. This board was the first iteration of the PCB that was manufactured to test the stimulator circuit, and has been used for testing since the remote implant was unavailable. The output from the stimulator module is displayed on the oscilloscope.
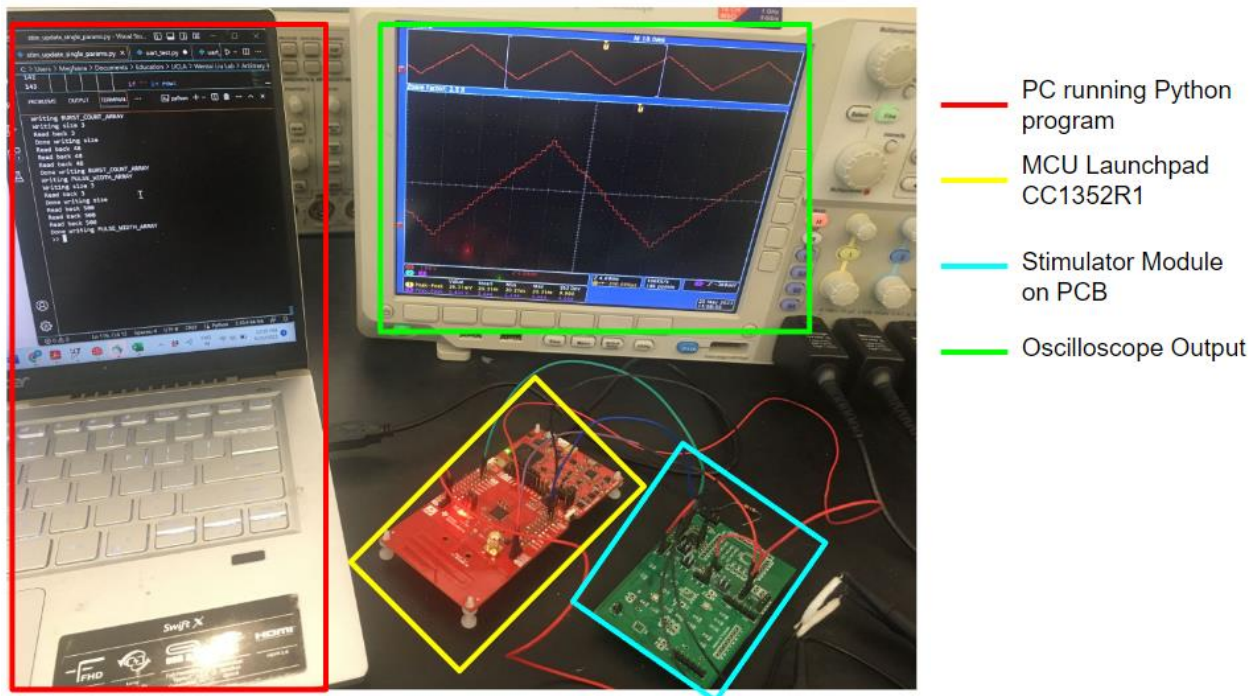
FIGURE 26. Test setup. The Python program sends UART data to the MCU on the launchpad (connected via USB). The MCU DAC and GPIO outputs go to the stimulator module. The output of the stimulator is displayed on the oscilloscope.

5.2 UPDATING STIMULATION PARAMETERS

The following sample waveforms have been generated from the MCU by updating stimulation parameters through a file.

RAMP WAVEFORM

Parameter	Values					
Amplitude	-20	20	-40	40	- - - -	240
Rest Period (µs)	2000					
Pulse Count	24					
Pulse Width (µs)	200					

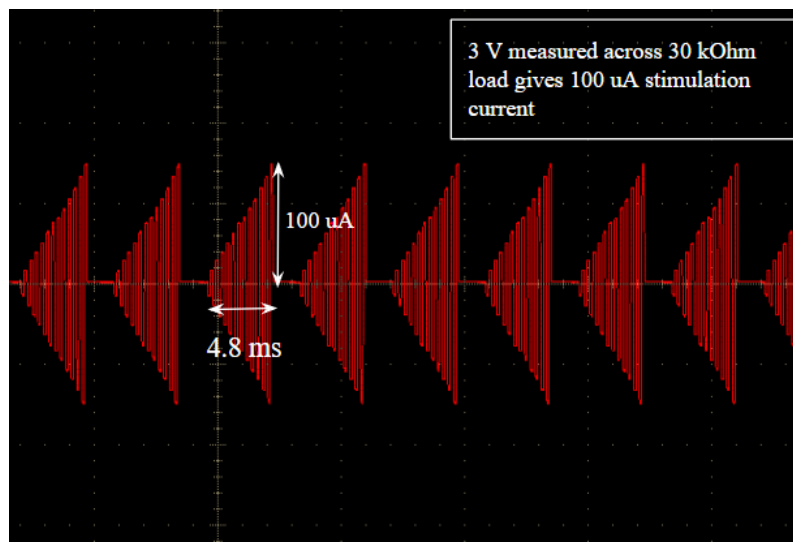**TABLE 5.** Ramp waveform stimulation parameters
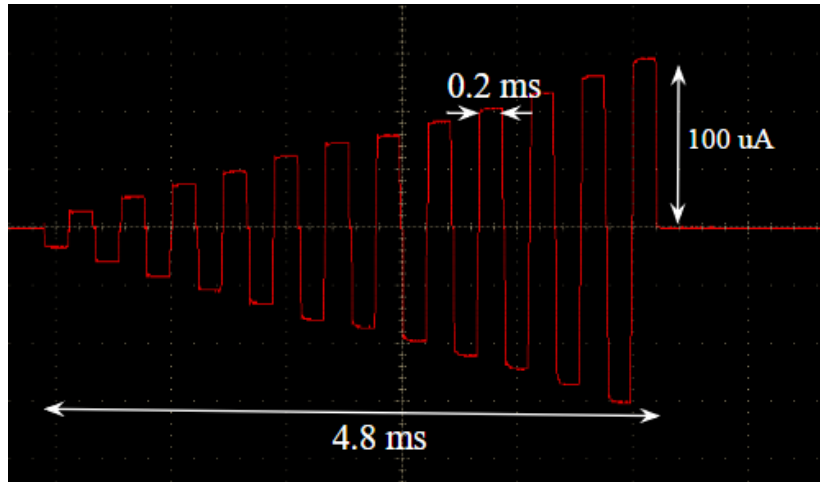

FIGURE 27. Ramp waveform image from oscilloscope.

FIGURE 28. Ramp waveform (zoomed-in) from oscilloscope.

SQUARE PULSES OF DECREASING INTER-PULSE DELAY

Parameter	Values					
Amplitude	-200	200	-200	-200	- - - -	220
Rest Period (µs)	20000					
Pulse Count	32					
Pulse Width (µs)	60					

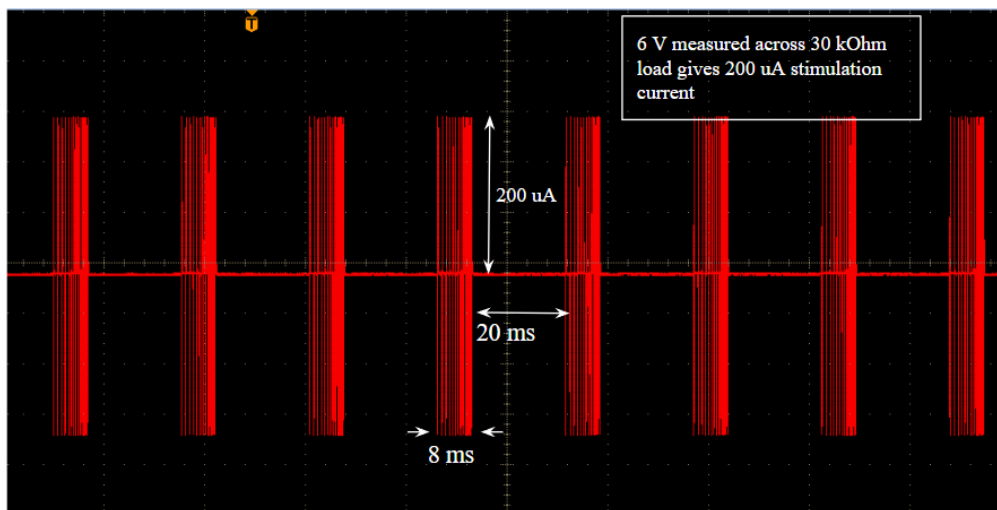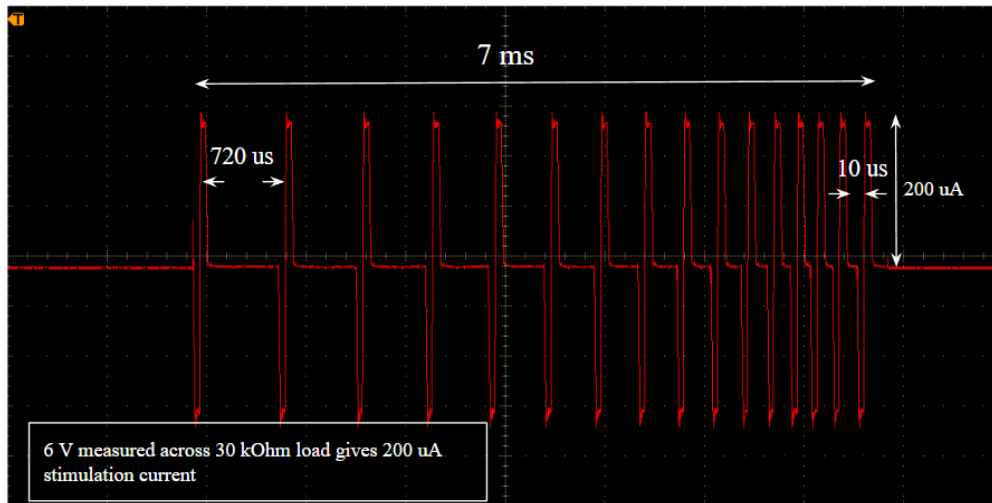**TABLE 6.** Square waveform stimulation parameters
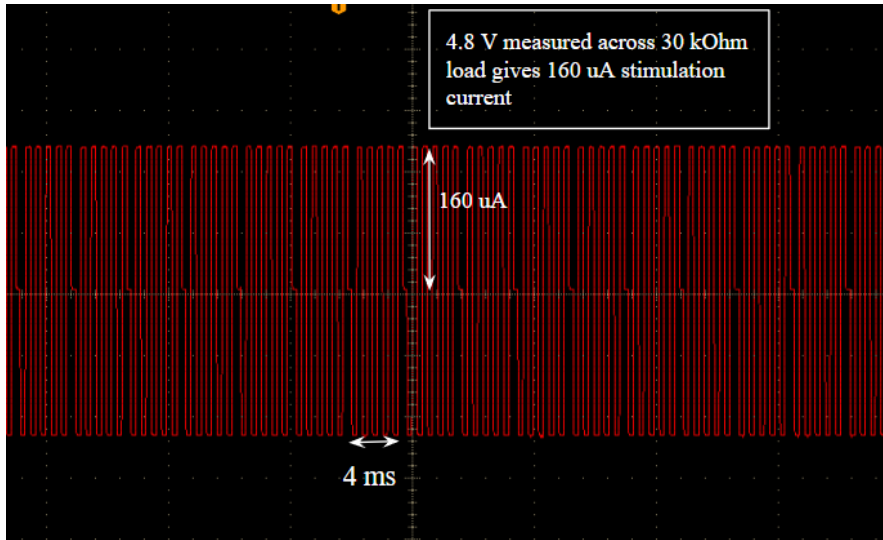

FIGURE 29. Square pulse waveform image from oscilloscope.

38

FIGURE 30. Square pulse (zoomed-in) image from oscilloscope.

HIGH FREQUENCY STIMULATION

Parameter	Values					
Amplitude	-200	200	-200	200	- - - -	200
Rest Period (µs)	15					
Pulse Count	100					
Pulse Width (µs)	400					

TABLE 7. 2.5kHz waveform stimulation parameters

39

FIGURE 31. High frequency 2.5kHz waveform image from oscilloscope.
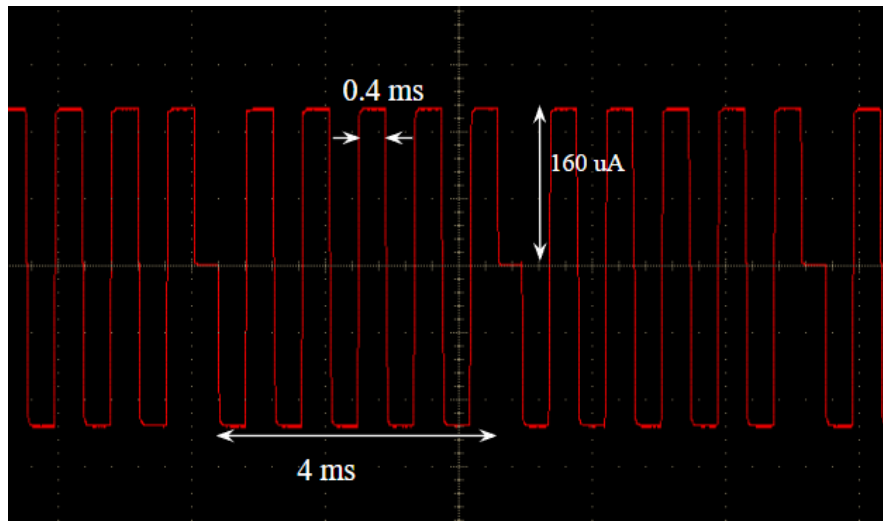
FIGURE 32. High frequency 2.5kHz waveform (zoomed-in) from oscilloscope.

Note: In this example of high frequency stimulation, a delay of around 400us exists between the two pulse trains. This is a known issue that exists because the firmware is organised as burst stimulation with a required minimum amount of rest period between bursts.

SINE WAVE

Parameter	Values				
Amplitude	0	16	32	48	- - - -	-17
Rest Period (µs)	15				
Pulse Count	100				
Pulse Width (µs)	167				

TABLE 8. Sine waveform stimulation parameters

FIGURE 33. Sine waveform image from oscilloscope.

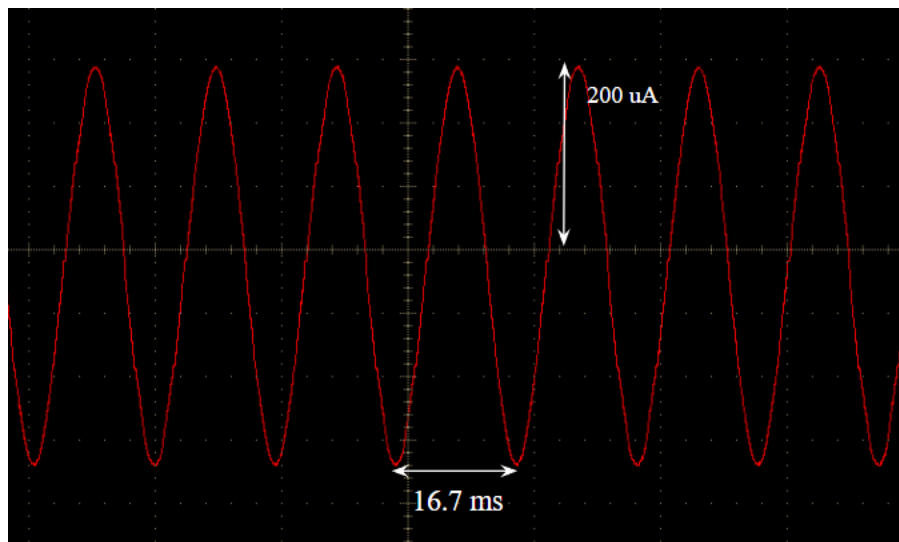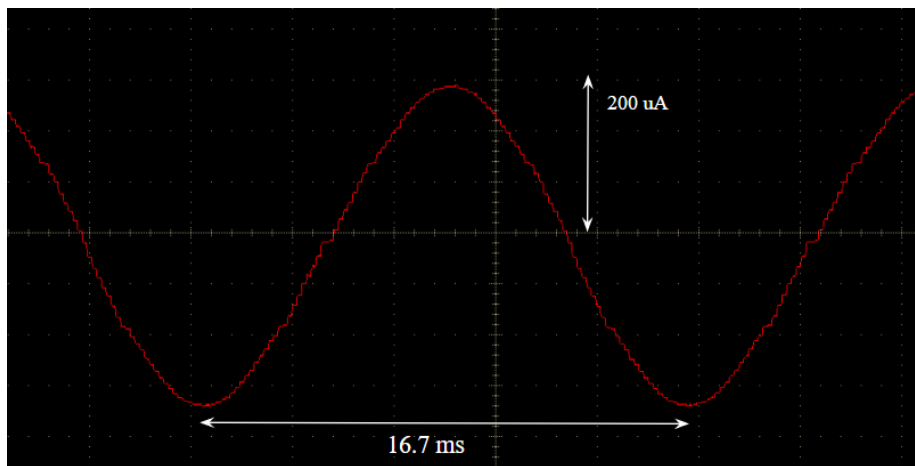**FIGURE 34.** Sine waveform (zoomed-in) image from oscilloscope.

TRIANGULAR WAVEFORM

Parameter	Values						
Amplitude	10	30	---	250	230	---	10
Rest Period (µs)	50						
Pulse Count	48						
Pulse Width (µs)	500						

TABLE 9. Triangular waveform stimulation parameters
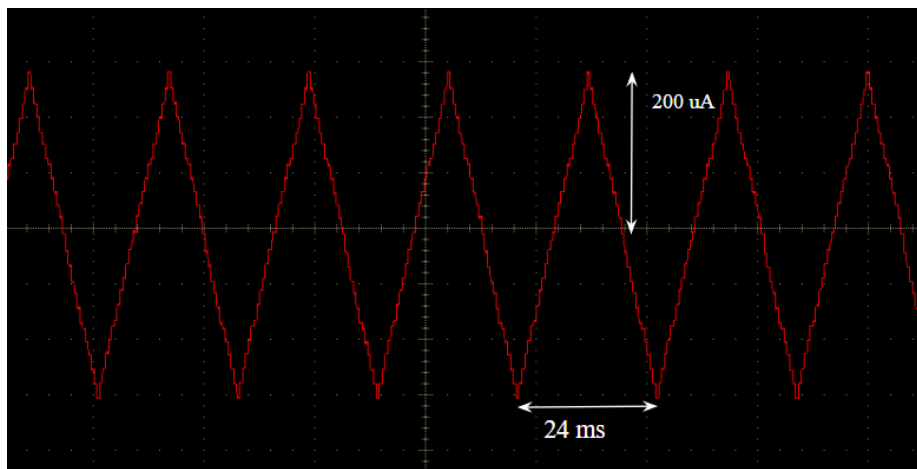
FIGURE 35. Triangular waveform image from oscilloscope.

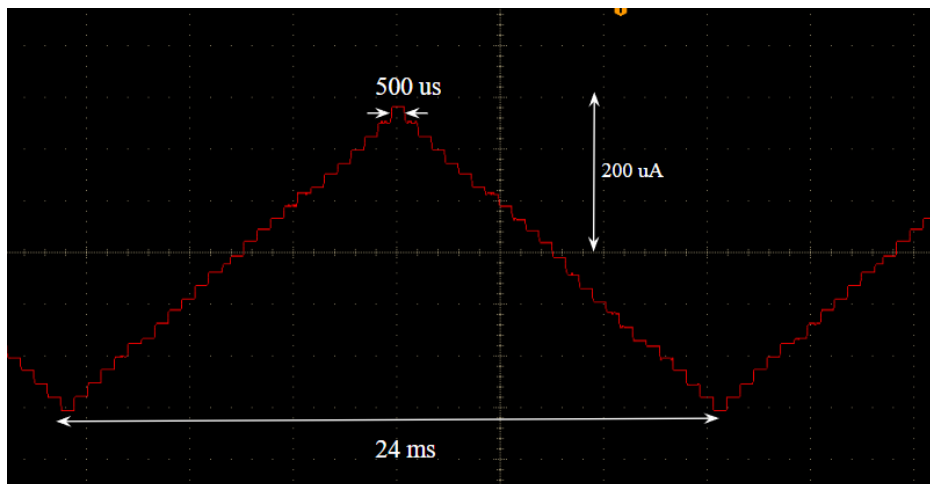**FIGURE 36.** Triangular waveform (zoomed-in) image from oscilloscope.

5.3 BIOMIMETIC SIGNAL TRANSFER

A file containing two EMG sessions of 30s was used. The data was collected at 0.5ms and the file consisted of 60000 datapoints in total.

For this test, the data was divided into blocks of 100 values each, or lengths of 50ms. The blocks were transferred one after the other. 10 blocks were transferred in total, giving a total EMG length of 0.5s. The block division is demonstrated in Figure 37.
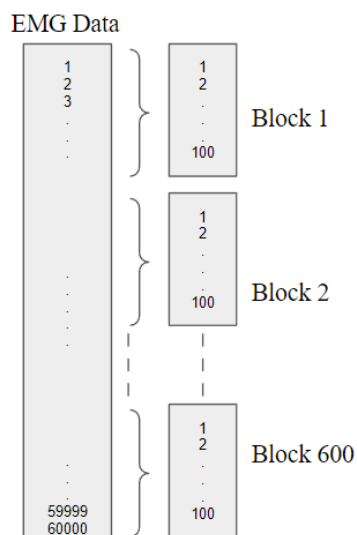
FIGURE 37. Division of EMG data into blocks of 100 values each.

The first EMG session is shown in Figure 38.
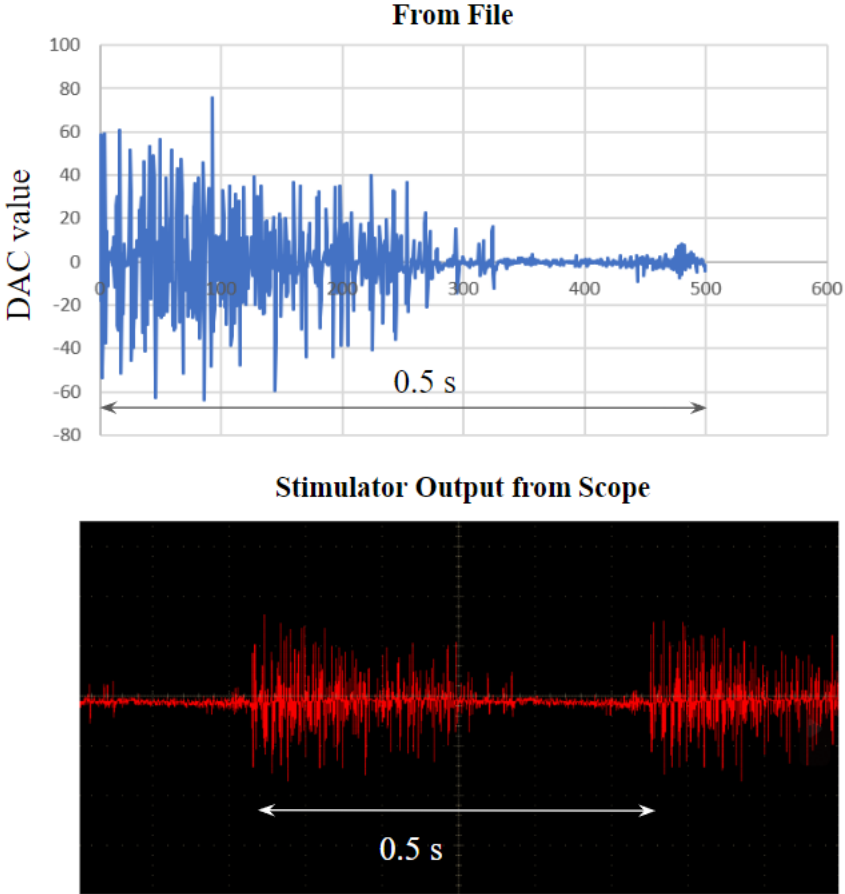
FIGURE 38. EMG Session-1. Comparison of EMG data between the waveform data from the file and the oscilloscope output for the first 0.5s (1000 samples).

The second EMG session is shown in Figure 39.
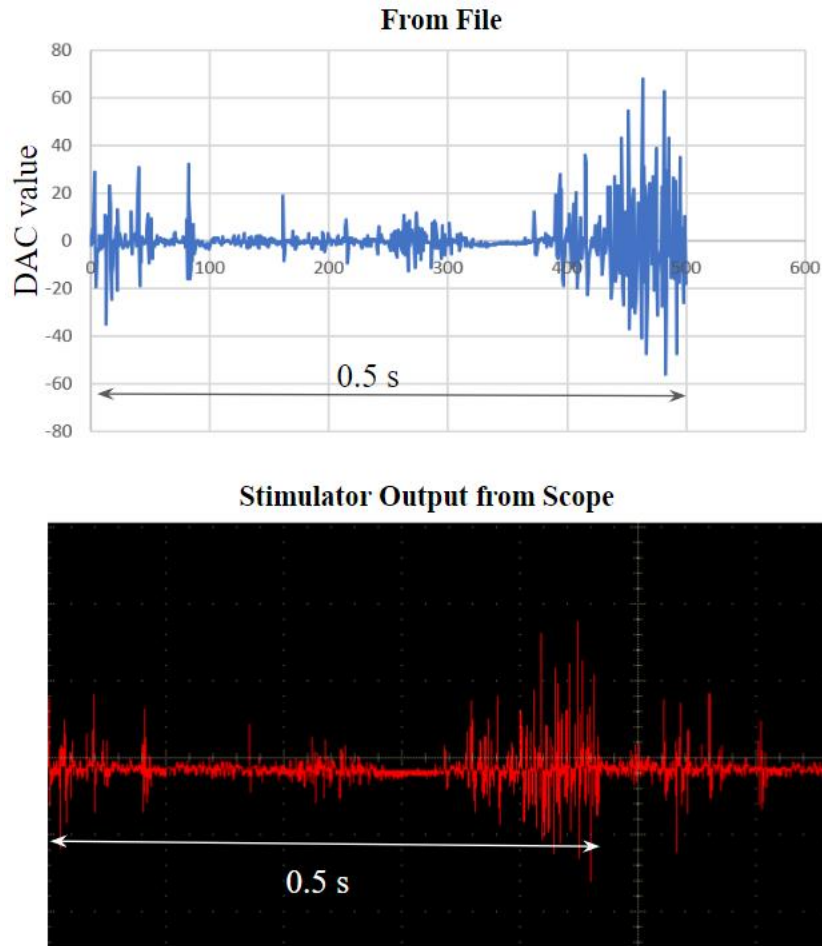
FIGURE 39. EMG Session -2. Comparison of EMG data between the waveform data from the file and the oscilloscope output for the first 0.5s (1000 samples).

The total time taken for an EMG of 0.5s to transfer into the UART is 5s. This is due to the need for a programmed delay between the sending of each block of data. The delay is currently set to 0.5s. It was observed that reducing the delay below this value results in a distortion of the output of the stimulator. This distortion arises because the delivery of a large number of values (100 in this case) in a rapid sequence overloads the MCU, resulting in the creation of junk values in the UART buffer.

CHAPTER 5: LIMITATIONS AND FUTURE WORK

5.1 LIMITATIONS

As demonstrated in Chapter 4, if the delivery of an EMG signal of 0.5s takes 5 seconds, then 30s of EMG data would take 300 seconds, or 5 minutes. This is much too long for dynamic stimulation since the ultimate goal would be to update stimulation signals within a few milliseconds during closed loop control.

5.2 FUTURE WORK

MINIATURISED REMOTE UNIT

1. Currently, the miniaturised remote unit exists as a PCB render. Once the board has been manufactured and its components have been assembled, the entire unit needs to be tested to ensure functionality and signal integrity.

2. After the board has cleared its functional tests, the design for the packaging and the electrodes can be developed. The goal is for the entire system to weigh less than 2g, and have less than 34 mm^3 of volume.

DYNAMIC STIMULATION

1. Optimisation of the delay between the transmission of each block. Ideally, this delay should be less than 50ms, as this is the duration of 100 EMG datapoints. It was observed that the reduction in the size of each block enabled a reduction in the programmed delay. Further testing is required to determine the least number of values that can be sent to reduce this programmed delay to 50ms.

2. Convert the launchpad into a UART adapter or use another device like FT2232H.

3. Once the dynamic update of stimulation can take place almost instantaneously, this feature can be used to develop a closed loop control of the stimulation, by using signals read by the recorder to set the stimulation dynamically.

REFERENCES

1. Sisterson ND, Wozny TA, Kokkinos V, Constantino A, Richardson RM. Closed-Loop Brain Stimulation for Drug-Resistant Epilepsy: Towards an Evidence-Based Approach to Personalized Medicine. Neurotherapeutics. 2019 Jan;16(1):119-127. doi: 10.1007/s13311-018-00682-4. PMID: 30378004; PMCID: PMC6361057.

2. Benabid AL, Pollak P, Gervason C, Hoffmann D, Gao DM, Hommel M, Perret JE, de Rougemont J. Long-term suppression of tremor by chronic stimulation of the ventral intermediate thalamic nucleus. Lancet. 1991 Feb 16;337(8738):403-6. doi: 10.1016/0140-6736(91)91175-t. PMID: 1671433.

3. Campbell JN, Long DM. Peripheral nerve stimulation in the treatment of intractable pain. J Neurosurg. 1976 Dec;45(6):692-9. doi: 10.3171/jns.1976.45.6.0692. PMID: 1086348.

4. Taccola G, Sayenko D, Gad P, Gerasimenko Y, Edgerton VR. And yet it moves: Recovery of volitional control after spinal cord injury. Prog Neurobiol. 2018 Jan;160:64-81. doi: 10.1016/j.pneurobio.2017.10.004. Epub 2017 Nov 2. PMID: 29102670; PMCID: PMC5773077.

5. Weiland JD, Liu W, Humayun MS. Retinal prosthesis. Annu Rev Biomed Eng. 2005;7:361-401. doi: 10.1146/annurev.bioeng.7.060804.100435. PMID: 16004575.

6. Moore DR, Shannon RV. Beyond cochlear implants: awakening the deafened brain. Nat Neurosci. 2009 Jun;12(6):686-91. doi: 10.1038/nn.2326. Epub 2009 May 26. PMID: 19471266.

7. Birmingham K, Gradinaru V, Anikeeva P, Grill WM, Pikov V, McLaughlin B, Pasricha P, Weber D, Ludwig K, Famm K. Bioelectronic medicines: a research roadmap. Nat Rev Drug Discov. 2014 Jun;13(6):399-400. doi: 10.1038/nrd4351. PMID: 24875080.

8. Shealy CN, Mortimer JT, Reswick JB. Electrical inhibition of pain by stimulation of the dorsal columns: preliminary clinical report. Anesth Analg. 1967 Jul-Aug;46(4):489-91. PMID: 4952225.

9. Wall PD, Sweet WH. Temporary abolition of pain in man. Science. 1967 Jan 6;155(3758):108-9. doi: 10.1126/science.155.3758.108. PMID: 6015561.

10. Caylor, J., Reddy, R., Yin, S. *et al.* Spinal cord stimulation in chronic pain: evidence and theory for mechanisms of action. *Bioelectron Med* **5**, 12 (2019). https://doi.org/10.1186/s42234-019-0023-1

11. Cracchiolo M, Ottaviani MM, Panarese A, Strauss I, Vallone F, Mazzoni A, Micera S. Bioelectronic medicine for the autonomic nervous system: clinical applications and perspectives. J Neural Eng. 2021 Mar 17;18(4). doi: 10.1088/1741-2552/abe6b9. PMID: 33592597.

12. Miller JP, Eldabe S, Buchser E, Johanek LM, Guan Y, Linderoth B. Parameters of Spinal Cord Stimulation and Their Role in Electrical Charge Delivery: A Review. Neuromodulation. 2016 Jun;19(4):373-84. doi: 10.1111/ner.12438. Epub 2016 May 6. PMID: 27150431.

13. Charles C. Horn, Jeffrey L. Ardell, and Lee E. Fisher. Electroceutical Targeting of the Autonomic Nervous System. Physiology 2019 34:2, 150-162. doi: 10.1152/physiol.00030.2018

14. Ayton LN, Barnes N, Dagnelie G, Fujikado T, Goetz G, Hornig R, Jones BW, Muqit MMK, Rathbun DL, Stingl K, Weiland JD, Petoe MA. An update on retinal prostheses. Clin Neurophysiol. 2020 Jun;131(6):1383-1398. doi: 10.1016/j.clinph.2019.11.029. Epub 2019 Dec 10. PMID: 31866339; PMCID: PMC7198351.

15. Tsaava, T., Datta-Chaudhuri, T., Addorisio, M.E. *et al.* Specific vagus nerve stimulation parameters alter serum cytokine levels in the absence of inflammation. *Bioelectron Med* **6**, 8 (2020). https://doi.org/10.1186/s42234-020-00042-8

16. L. A. Geddes and J. D. Bourland, "The Strength-Duration Curve," in *IEEE Transactions on Biomedical Engineering*, vol. BME-32, no. 6, pp. 458-459, June 1985, doi: 10.1109/TBME.1985.325456.

17. Tasaki. (1953). Nervous transmission. Thomas

18. HODGKIN, A., HUXLEY, A. Action Potentials Recorded from Inside a Nerve Fibre. *Nature* **144**, 710–711 (1939). https://doi.org/10.1038/144710a0

19. Warren M. Grill. Chapter 7 - Model-based analysis and design of waveforms for efficient neural stimulation. Progress in Brain Research, Volume 222, 2015, Pages 147-162. https://doi.org/10.1016/bs.pbr.2015.07.031.

20. Datta-Chaudhuri, T. Closed-loop neuromodulation will increase the utility of mouse models in Bioelectronic Medicine. *Bioelectron Med* **7**, 10 (2021). https://doi.org/10.1186/s42234-021-00071-x

21. Angotzi, G., Boi, F., Zordan, S. *et al.* A programmable closed-loop recording and stimulating wireless system for behaving small laboratory animals. *Sci Rep* **4**, 5963 (2014). https://doi.org/10.1038/srep05963

22. Deshmukh A, Brown L, Barbe MF, Braverman AS, Tiwari E, Hobson L, Shunmugam S, Armitage O, Hewage E, Ruggieri MR Sr, Morizio J. Fully implantable neural recording and stimulation interfaces: Peripheral nerve interface applications. J Neurosci Methods. 2020 Mar 1;333:108562. doi: 10.1016/j.jneumeth.2019.108562. Epub 2019 Dec 17. PMID: 31862376.

23. Culaclii, S., Wang, P. M., Taccola, G., Yang, W., Bailey, B., Chen, Y. P., ... & Liu, W. (2021). A Biomimetic, SoC-Based Neural Stimulator for Novel Arbitrary-Waveform Stimulation Protocols.Frontiers in Neuroscience, 943. doi: 10.3389/fnins.2021.697731

24. Nong, Y. (2022). A Programmable Wireless Single Channel Neural Interface with Artifact Cancellation Capability. *UCLA*. ProQuest ID: Nong_ucla_0031N_20977. Merritt ID: ark:/13030/m56n0brs. Retrieved from https://escholarship.org/uc/item/9wd786qm

25. Scott F. Lempka, Cameron C. McIntyre, Kevin L. Kilgore, Andre G. Machado; Computational Analysis of Kilohertz Frequency Spinal Cord Stimulation for Chronic Pain Management. *Anesthesiology* 2015; 122:1362–1376 doi: 10.1097/ALN.0000000000000649

26. Spiral PCB coil inductance calculator. https://coil32.net/pcb-coil.html

27. Microstrip impedance calculator. https://cecas.clemson.edu/cvel/emc/calculators/PCB-TL_Calculator/microstrip.html